2011

Imaging Long-range Orientational Order In Monolayers Of Amphiphilic Molecules With Scanning Probe Force Microscope And Liquid Crystal Optical Amplification

Wenlang Liang
University of Central Florida

IMAGING LONG-RANGE ORIENTATIONAL ORDER IN MONOLAYERS OF AMPHIPHILIC MOLECULES WITH SCANNING PROBE FORCE MICROSCOPE AND LIQUID CRYSTAL OPTICAL AMPLIFICATION

by

WENLANG LIANG

B.S, Materials Processing and Control, 2008, Wuhan, Huazhong University of Science and Technology

A thesis submitted in partial fulfillment of the requirements

for the degree of Master of Materials Science and Engineering

in the Department of Mechanical, Materials and Aerospace Engineering

in the College of Engineering and Computer Science

at the University of Central Florida

Orlando, Florida

Fall Term

2011

ABSTRACT

Monolayers of amphiphilic molecules at interface provide a unique system for understanding the thermodynamic and rheological properties of quasi two-dimensional systems. They are also an excellent model accessible for studying cell membranes. The feature of long-range organization of molecular tilt azimuth in monolayers at the air/water interface is one of the most interesting findings over the past two decades, which leads to the formation rich and defined textures. By observing the changes in these textures, the transitions between tilted monolayer phases can be detected.

We study the boojum and stripe textures formed in the liquid-condensed phase of pentadecanoic acid (PDA) monolayers at the air/water interface and find that they can be preserved after being transferred to glass substrates at low dipping speeds at a temperature lower than the room temperature. Frictional force microscopy confirms the long-range tilt order in the transferred boojums and stripes of PDA, implying the interaction of the PDA molecules with the glass surface does not change the tilt order. Polymerized stripe textures of pentacosadiynoic acid (PCA) monolayers can also be transferred onto solid substrates. Atomic force microscopy shows that the PCA stripe textures represent the regular variations of molecular packing densities in PCA monolayers. Furthermore, we find that the molecular orientation and packing density changes in monolayers can induce the local order of nematic liquid crystals. Due to the long-range orientation correlation of nematic liquid crystals, the boojum and stripe textures in monolayers can be observed by an optical microscope after liquid crystal optical amplification.

Dedicated to

My family

ACKNOWLEDGMENTS

First and foremost, I would like to take this opportunity to express my gratitude to Dr. Jiyu Fang for his help, support and valuable discussions throughout my research. It has been an honor to be his student. His constant guidance and persistent spirit helped me substantially in the research work. I would also like to thank Dr. Linan An, Dr. Weiwei Deng and Dr. Qun Huo for serving on my thesis committee and for their encouragement and insightful comments.

Specially thanks Xuejun Zhang for helping me a lot in the lab. I thank my friends, Jianhua Zou and Tanmay Bera for their help and support.

I would like to thank my parents, brother, sister-in-law and my niece for their love and encouragement.

TABLE OF CONTENTS

LIST OF TABLES

LIST OF FIGURES

CHAPTER 1. INTRODUCTION

1.1 Langmuir-Blodgett Films

Langmuir-Blodgett (LB) films can be defined as mono-molecular assemblies on substrates. Irving Langmuir is regarded as the father figure in this field. Langmuir discovered the forces between molecules were short range and acted only between molecules in contact with monolayer films, and laid down the fundamental scientific foundation of mono-molecular films[1]. He described the surface effect of the mono-molecular in *The Constitution and Fundamental Properties of Solids and Liquids* in 1917, in which he studied the pressure-area property of molecules in the subphase[2]. His research showed the hydrophilic head groups were the only part immersed in the subphase of acids, alcohols and esters. Katherine Blodgett developed the technique of transferring the films onto solid substrates. This technique can be used as transferring a monolayer film, as well as building up multilayer films. And this technique is generally known as the Langmuir-Blodgett technique. Figure 1 gives us an idea of what does the NIMA LB trough look like.

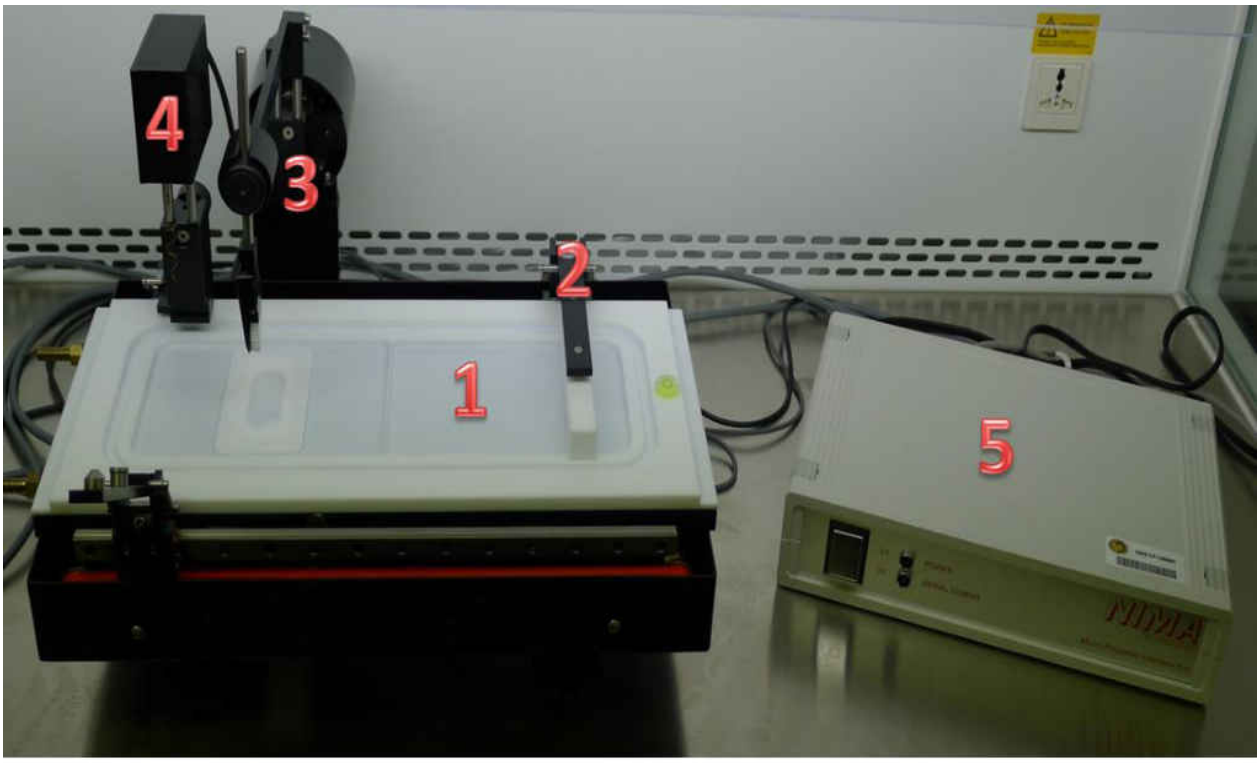

(1) Trough top (2) Barrier (3) Dipping mechanism
(4) Surface pressure sensor (5) Interface Unit

Figure 1 NIMA Langmuir-Blodgett Deposition Trough.

The way to produce LB films is by spreading solution onto the subphase and later on transferred to solid substrates. There are a few factors needed to be taking into consideration. First is choosing the solvent. Solvent must be volatile, chemically inert with respect to the solute and also needs to be relatively pure. To test the purity of the solvent, one can use the "Blank Spreading" technique [2], which is by spreading the solvent onto the subphase, giving it time to evaporate and then runs an isotherm. If surface pressure remains unchanged, the solvent is qualified to use. The volatility of the solvent should neither be too long nor too short. Second is spreading. Syringe is preferred to be used as the spreading tool. The distance between the

subphase and the needle should be within several millimeters, and each drop should be allowed to evaporate before the next is applied. Third is substrate. Substrate must be thoroughly cleaned as it determines the property of the first layer. Substrates can be generally divided into two type base on the surface property: hydrophobic and hydrophilic. Figure 2 shows how the molecules of the first layer will arrange when transferred on to a hydrophilic substrate.

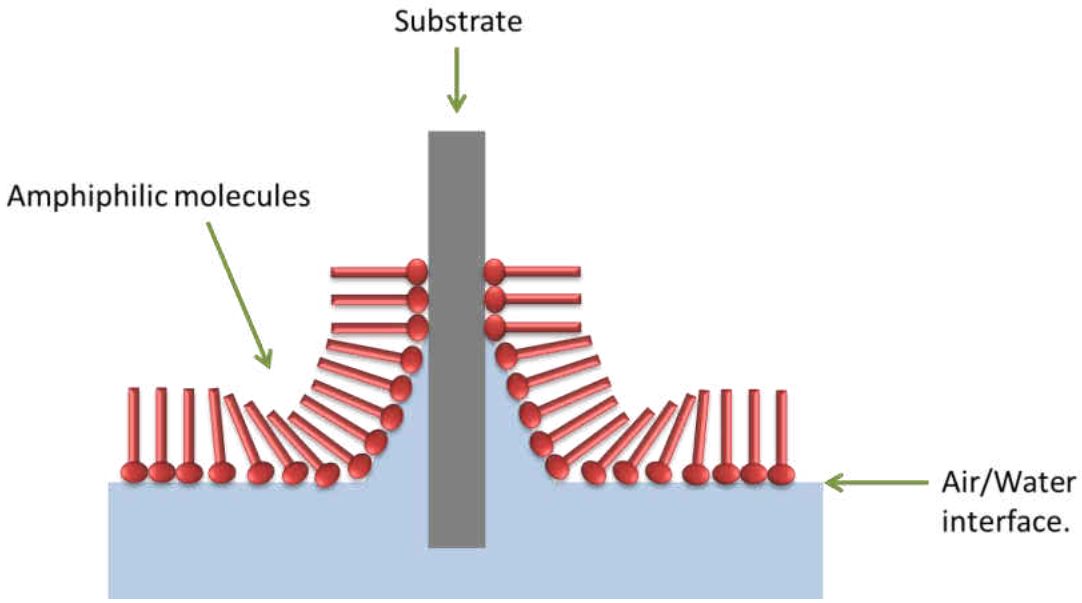

Figure 2 Deposition of the first monolayer onto a hydrophilic substrate.

In the subphase, surface tension will bring the peripheral molecules into the bulk, and the tendency of surface-active molecules to accumulate at the interface favors expansion of the interface to lower the surface tension. The reduction of surface tension is called surface pressure. Base on this phenomenon and given the number of molecules on the surface is known, it is possible to monitor the surface pressure as a function of the area occupied per molecule. The NIMA LB trough uses the Wilhelmy plate method to measure surface tension. The Wilhelmy

plate is made from a strip of chromatography paper. At constant temperature, the plot of surface pressure as a function of the area occupied per molecule is known as the pressure/area isotherm, which is usually abbreviated to isotherm.

Figure 3 is a typical LB trough compression isotherm. Normally there are four phases of the isotherm: gaseous phase, liquid expanded (LE) phase, coexistence phase and liquid condensed (LC) phase.

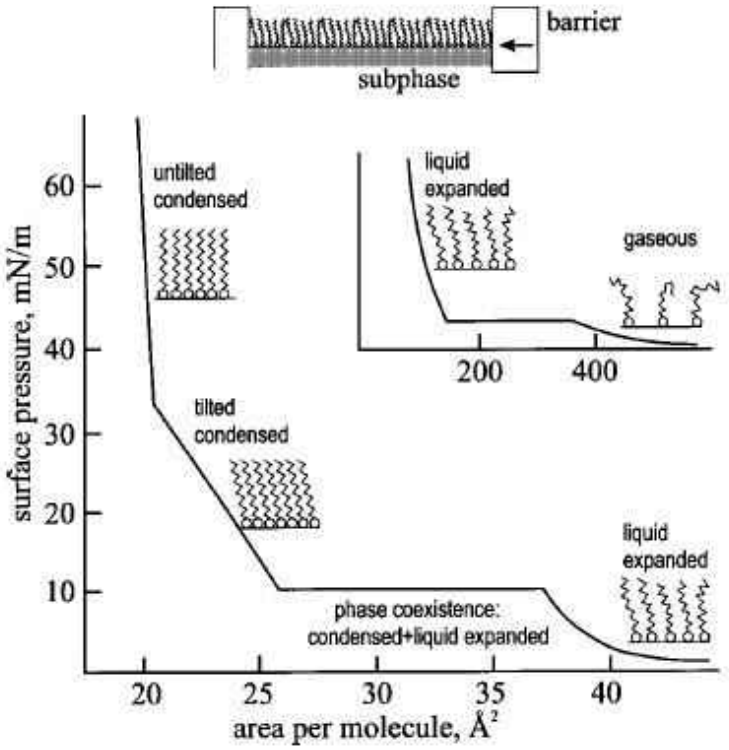

Figure 3 Schematic diagram of typical LB trough compression isotherm (ref. 3).

1.2 Monolayers

Monolayers at the air/water interfaces and Langmuir-Blodgett (LB) monolayers on solid substrates of amphiphilic molecules have been studied for a century. Nonetheless, the monolayer systems still attract great interest, due to the fact that they are distinctive models to the study of cell membranes[4-10] and also contribute to better understanding of the thermodynamic and theological properties of quasi two-dimensional systems[11-18]. Technological potential of aligning monolayers on solid substrates have been presented in molecular electronics, sensors and nonlinear optics[19-20]. Long-range orientational order and short-range positional order was discovered during the past two decades[3, 21]. Tilted molecules with respect to the surface normal of several long-range ordered phases have been shown by grazing incidence X-ray diffraction; regarding to the underlying bond orientational order, the tilt azimuth has a well-defined orientation[22]. In the tilted phases of fatty acids, esters and lipids, well defined and rich optical textures have been discovered, such as mosaic[23-26], star[27-28], Stripe[29-30], and boojum[31], which all represent large-scale self-organization of the molecular tilt azimuth. Landau-deGennes theory of tilted hexatic phases that takes into account the broken-symmetry characteristic of amphiphiles at the air/water interface can explain most of these textures[32-33].

1.3 Brewster Angle Microscope

BAMs are primary designed to visualize Langmuir films and the tilted phases at the air-water interface[24]. When p-polarized light is projected to pure water at an incident angle $\propto$ of 53.1°, there will be no reflection and the image of BAM under this condition is black. This angle is known as the Brewster angle. When the incident light hits other materials, the refractive index

changes and the reflected light will form an image. The brightness of the image varies, depending on the molecular arrangement and densities at the interface.

Plenty of works have been done within the coexistence phase range. Boojums[31], stars[27-28] and other patterns[24-26, 29-30] of fatty acids, esters and lipids had been discovered in the tilted phases at the air/water interface, mostly by Brewster Angle Microscope (BAM).

BAM is a well-developed technology and has been widely used. However the drawback of BAM is it could be only used to characterize surface at the interface. In order to have a better understanding of the LB monolayers in the coexistence phase, we decided to use liquid crystal (LC) and atomic force microscope (AFM) to image and analyze the transferred LB monolayers on substrates.

1.4 Atomic Force Microscope

The Atomic force microscope (AFM) can provide accurate resolution image on the surface, analyze and characterize materials at nanoscales. In 1985 Gerd Binning brought up the concept of using force instead of electric current to image a surface. With the help and C. Gerber and C. Quate, they made the first prototype of atomic force microscopy[34]. Figure 4 shows a schematic of the components of AFM. The tip is mounted on the end of a cantilever spring, laser beam is used to detect the deflection of the cantilever, the feedback electronic system will transfer data to the computer, and the display system will convert the data to images.

When the tip is brought very close to the sample surface, the interaction between the surface and the tip will deflect the cantilever. The deflection of the cantilever detected by the

laser beam will transfer to the feedback electronic system and then reach the computer system which converts the data into an image of the sample surface.

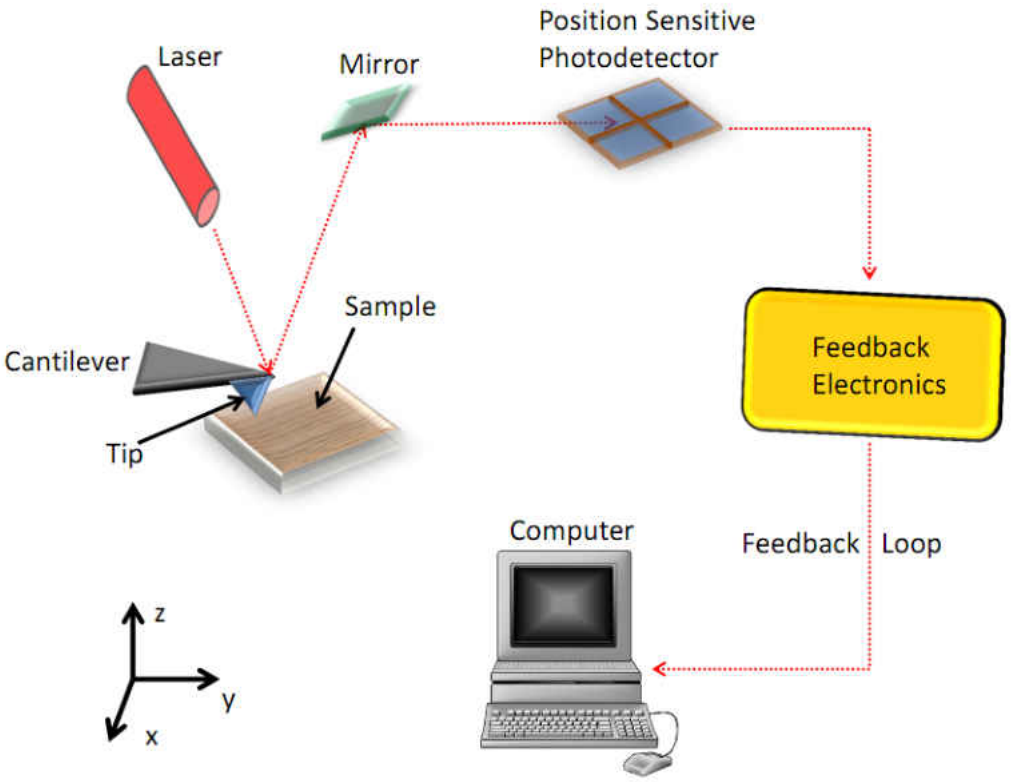

Figure 4 Schematic components and operation of AFM.

1.4.1 Force Distance Curves

The force distance curve indicates the relationship between the position of the tip and the force. When the tip is approaching the sample surface, at first there is only small repulsive force because of the attractive surface forces. As the tip moves forward towards the sample surface, the cantilever bends due to the interaction with the surface, therefore the force increases. The tip continues to move to the preset sample surface position, and then moves backwards. Finally the tip returns to its original position. The force distance curve is shown in Figure 5.

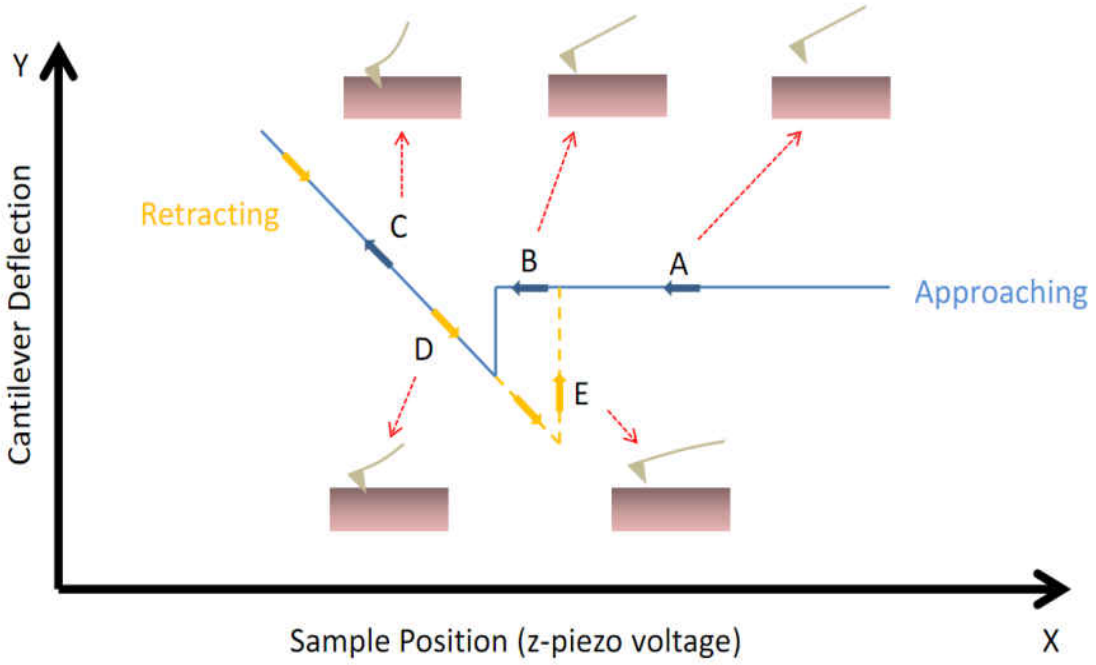

Figure 5 Schematic of AFM force distance curve.

1.4.2 Operation Modes of AFM

There are three primary operating modes regarding to the interaction between the tip and sample materials.

(1) Contact Mode

Under this mode, the tip keeps close and "soft" physical contact with the sample surface. Due to the surface profile of the sample, cantilever deflection changes. Using a feedback loop to keep the cantilever deflection constant by changing piezo-voltages, therefore by collecting the

piezo-voltages an image is obtained. The advantages of contact mode are it can achieve high scan speed; also it is the only mode that can obtain atomic resolution images; and it is easier to scan the changes in topography when it comes to rough surface samples. However, due to the high lateral and normal forces, soft samples like polymers can be damaged.

(2) Tapping Mode

The cantilever is oscillated near its resonant frequency and remains the oscillation amplitude constant. By maintaining a constant interaction between the tip and sample, images are obtained. The advantages of tapping mode are it can achieve high lateral resolution; no lateral forces hence very little damage to the samples; and when compared to the non-contact mode, the imaging condition is more stable. But the scan speed in the tapping mode is lower when compared to contact mode. Also the normal forces are larger than the non-contact mode.

(3) Non-Contact Mode

The tip does not contact with the sample and the cantilever is oscillated above its resonant frequency. The attractive forces (Van der Waals forces) change the amplitude, and by maintaining the amplitude constant, images are obtained. The advantages of non-contact mode are the lateral and normal forces are lower, therefore is less damaged to the soft samples. The disadvantages are when compared to contact mode, the scan speed is lower; and the imaging conditions are unstable.

The images in this thesis were taken from tapping mode and contact mode.

1.5 Liquid Crystal

Liquid crystals are highly anisotropic fluids, in which molecules have long-range orientational order, but little positional order. This unique feature places liquid crystals between crystals (which possess both positional and orientational order) and isotropic fluids (which exhibit no long-range order). Figure 6 shows schematic of molecules alignment of solid state, liquid crystal state and liquid state. Possessing the internal order and coherence of crystals, with the fluidity of liquids, permits liquid crystals to act as a sensitive material. The energy required to perturb the molecular order of liquid crystals is very small, and any defect or non-uniformity of the surface in contact with the liquid crystals leads to changes in the local order [35-36]. The surface-induced changes in the molecular order can extend over tens of micrometers into the bulk liquid-crystal phase on time scales of milliseconds. This in turn leads to observable optical patterns or textures in a polarizing optical microscope ("optical amplification").

The liquid crystal phase is first discovered by Friedrich Reinitzer[37]. Figure 7 schematic of structures of liquid crystal molecules. As noticed that the cholesteryl benzoate had two distinct melting points, he designed the experiment to increase the temperature of a solid cholesteryl benzoate sample and observed the solid changed into hazy liquid. As the temperature kept increasing, the hazy liquid slowly changed to clear and transparent liquid. Later Lehman[38] used polarizing microscope to observe liquid crystal, and discovered they exhibit crystalline optical properties but also had the viscous as liquid. And later the name "liquid crystal" was widely used.

Molecules in liquid phase are randomly ordered while in solid state they will be highly ordered. In liquid crystal state, the molecules are not perfectly ordered, but they have the director, which would orient the molecules to point along a certain preferred axis called director. The liquid crystal phase is also known as the mesogenic state[39, 40].

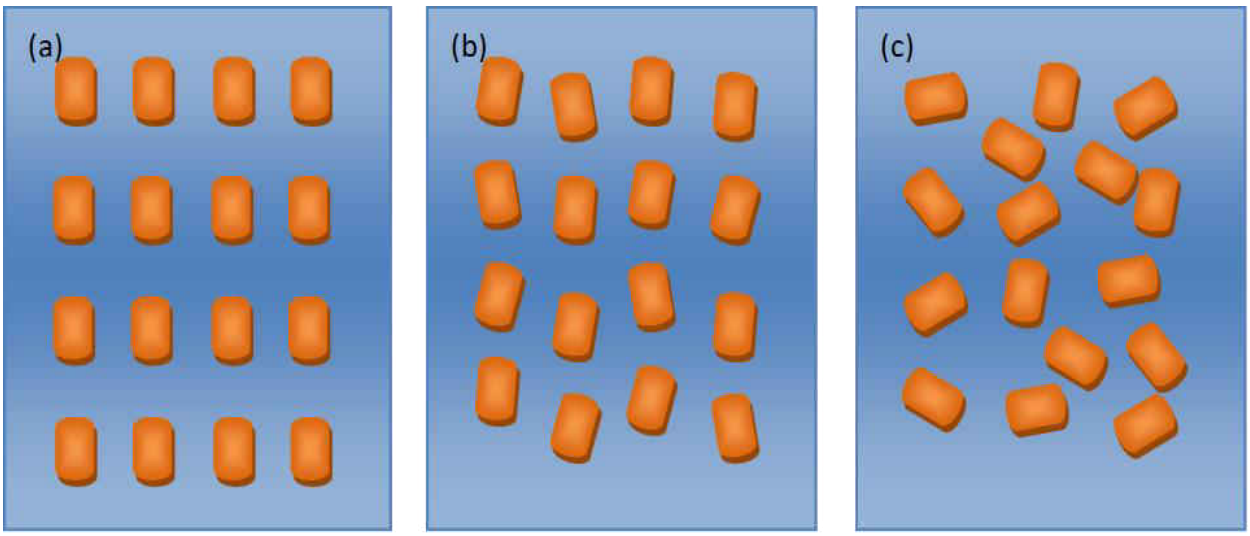

Figure 6 Schematic of molecules alignment of solid state (a), liquid crystal state (b) and liquid state (c).

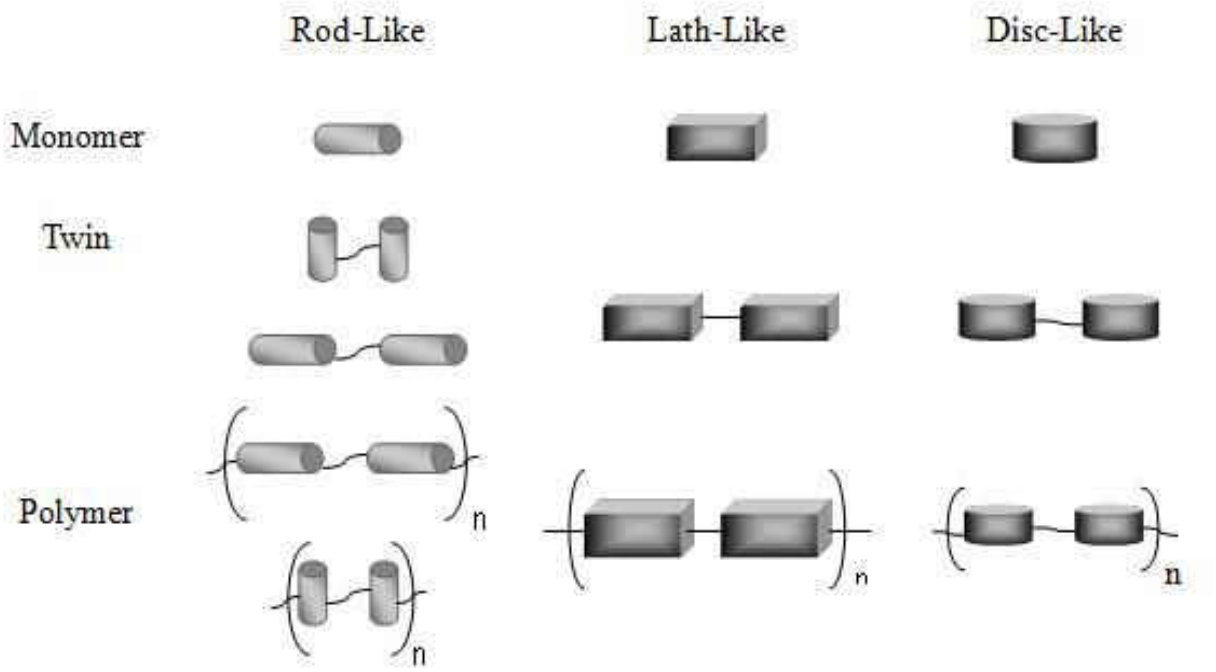

Figure 7 Schematic of structures of liquid crystal molecules.

The classical liquid crystals are derived from rod-like molecules. About 3/4 of the rod like mesogenic compounds are compiled in table books so far[41, 42]. Chandrasekhar et al. and Billard et al. discovered the liquid crystals originated from disc-like molecules[39, 40]. The lath like species of liquid crystal is the intermediate form between the rod like and the disc like forms.

Liquid crystals have intermediate physical properties between conventional solids and fluids, which exhibit structural orders in the arrangement of molecules while the physical form is like fluid. There are three types of liquid crystals, thermotropic, lyotropic and polymeric.

1.5.1 Thermotropic Liquid Crystal

Thermotropic liquid crystals are temperature dependent and have a series of phase transition occur over a temperature range. Enantiotropic liquid crystals are only stable above the melting point, while monotropic liquid crystals are only stable below the melting point and had to be using decreasing temperature method to acquire.

Friedel[43] classified thermotropic rod-like liquid crystals into three types based on the nomenclature, which are nematic, smectic and cholesteric. Table 1 shows the structures of thermotropic liquid crystals.

Phase Type	Structure
Nematic	Molecules are statistically oriented along a certain preferred axis n called director. The symmetry is not changed by the substitution. Nematic is nonpolar in the bulk
Cholesteric	The axis of orientation of the molecules rotates through an angle 360^{o} over the distance equal to the helix pitch P_o.
Smectic A	Molecules are arranged in layers perpendicular to the layer normal.
Smectic C	Molecules are arranged in layers oblique to the layer normal.

Table 1 Structures of thermotropic liquid crystals (ref. 44).

Lyotropic liquid crystals are usually obtained during the increase of concentration of isotropic solutions of certain materials in a suitable solvent, which are very concentration and temperature dependent. Usually the systems are formed by water and amphilhilic molecules. Lyotropic liquid crystals are of interest in biological studies[45].

The liquid crystals which can form both thermotropic as well as lyotropic states are called amphotropic. The amphotropic behavior can be found in polyhydroxy amphiphiles, disc like and rod like liquid crystals and block-copolymers[46].

Thermotropic liquid crystals are the most extensively studied, and their physical properties are depending on the temperature. As temperature increases, thermotropic liquid crystals would go through phase transitions from solid to liquid, then to isotropic liquid and in the end to vapor. Thermotropic liquid crystals have three phases: nematic, cholesteric and

smectic. Figure 8 shows the schematic of thermotropic liquid crystals phases: (a) nematic, (b) smectic A, (c) smectic C and (d) cholesteric.

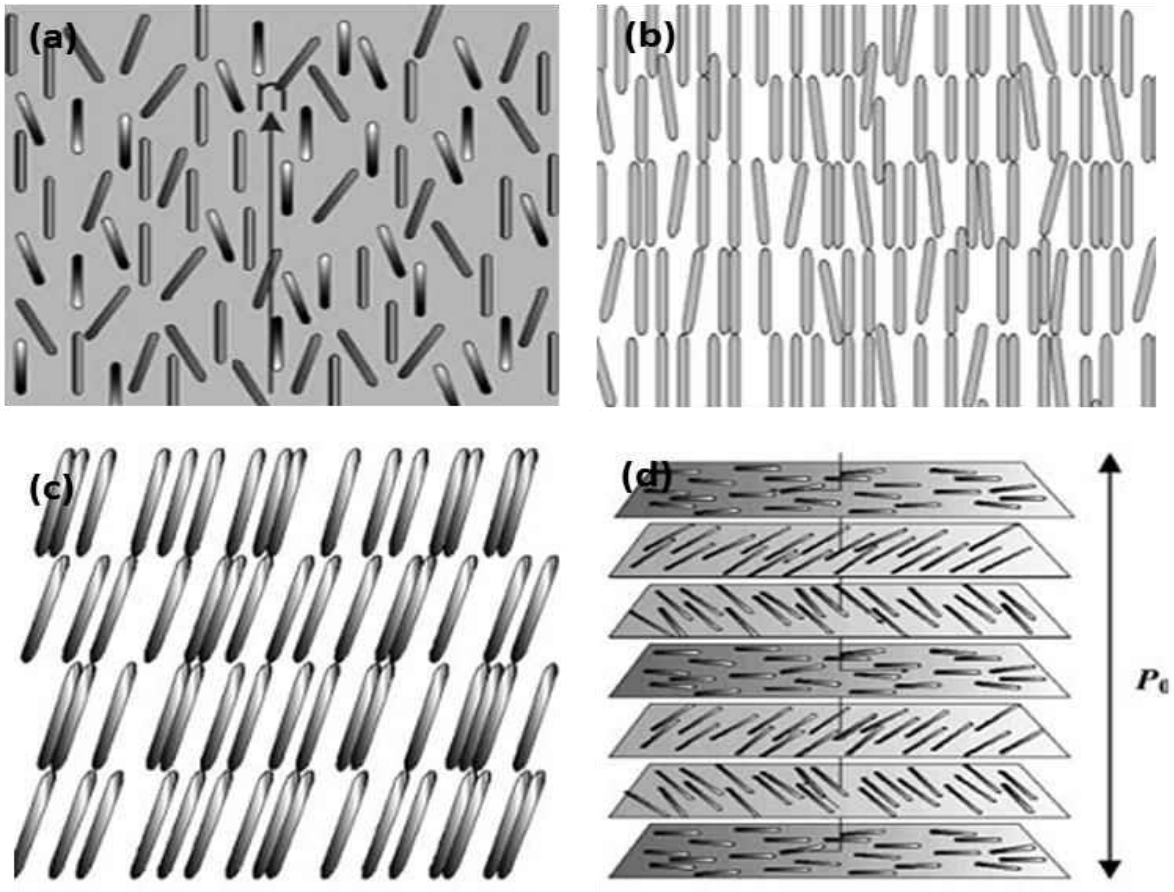

Figure 8 Schematic of thermotropic liquid crystals phases: (a) nematic, (b) smectic A, (c) smectic C and (d) cholesteric (ref. 47).

1.5.2 Nematic Phase

Liquid crystals in nematic phases have the same director, which means they intend to point to the same direction but are not positional ordered. The orientation of the director can change in space. However, the molecular dimension is much shorter than the characteristic distance of its variation, meaning that it is possible to create a uniform orientation molecular axis. Also the symmetry will not be changed by substitution. The order parameter of the nematic

phase is 0.7~0.8 and becomes zero when change into isotropic phase. The temperature of the phase transition between the nematic phase and isotropic phase is called clearing point.

Nematic liquid crystal molecules possess in a high degree of long range orientational order but do not have long range positional order, which is different with isotropic liquid molecules. X-Ray studies by Chistyakov[48] and Vries[49] showed some types of nematic liquid crystals have a lamellar type of short range order, containing cybotactic groups[50] formed by clusters of molecules.

The physical properties of nematic molecules are the same in the +**n** and –**n** directions along the axis director, indicating that they are centrosymmetric. If a permanent electric dipole is carried by each of the nematic molecules, the bulk dipole will vanish because of the way they assemble.

1.5.3 Smectic Phase

Some smectic liquid crystals, unlike nematic liquid crystals, are characterized by both the orientation and positional order, while others (e.g. hexatic phases) possess long range bond orientational order but no long range positional order[51]. The molecules position is correlated in certain ordered pattern, and all of the smectic molecules have a lamellar structure. There are several subphases of the smectic phase according to the ordering or arrangement of the molecules and structural symmetry properties[37, 49].

The smectic liquid crystals molecules are arranged in layers. The average thickness of the layers is related to the molecular length. Leadbetter[52] and Pershan[53] discovered several types of smectic modifications. The most commonly discussed smectic phases are smectic A and smectic C.

Recently, there has been an increased interest in using liquid-crystal optical amplification as a simple and fast imaging technique for studying the structures and amaproperties of organic and biological interfaces[54-63]. It has been demonstrated that liquid crystals can map differences in the spatial orientation of terminal groups in self-assembled monolayers (SAMs) formed from alkanethiols that differ by a single methylene[54]. The change in the spatial orientation between odd and even number of methylene groups in SAMs can cause a 90° rotation in the azimuthal orientation of liquid crystals. This information is not easily obtained by other imaging techniques. Nematic liquid crystal 5CB (4'-pentyl-4-cyanobiphenyl) could be employed as an optical amplification medium to image the seven-segment stars in the transferred monolayers of 1-monopalmitoyl-rac-glycerol that arise from variations in the molecular tilt azimuth[55].

The orientation of a nematic liquid crystal can be employed to image the textures that arise solely from the variation in the molecular tilt azimuth in both planar and cylindrical geometries. Liquid-crystal optical amplification is a fast and nondestructive method which can provide us a simple way to observe and characterize a number of important issues in monolayer studies.

1.6 Pentadecanoic acid and Pentacosadiynoic acid

Pentadecanoic acid (PDA) and 10, 12-pentacosadiynoic acid (PCA) Langmuir monolayers had been widely studied at the air-water interface. Figure 9 shows the molecular structures of PDA and PCA. Both PDA and PCA have a hydrophilic head group –COOH, and a long carbon chain which is hydrophobic. The significant difference between PDA and PCA, besides the number of carbon atoms, is that PCA has a diacetrylene group where polymerization

can be triggered. Monolayer of PDA and PCA molecules were transferred onto hydrophilic glass substrates in our study.

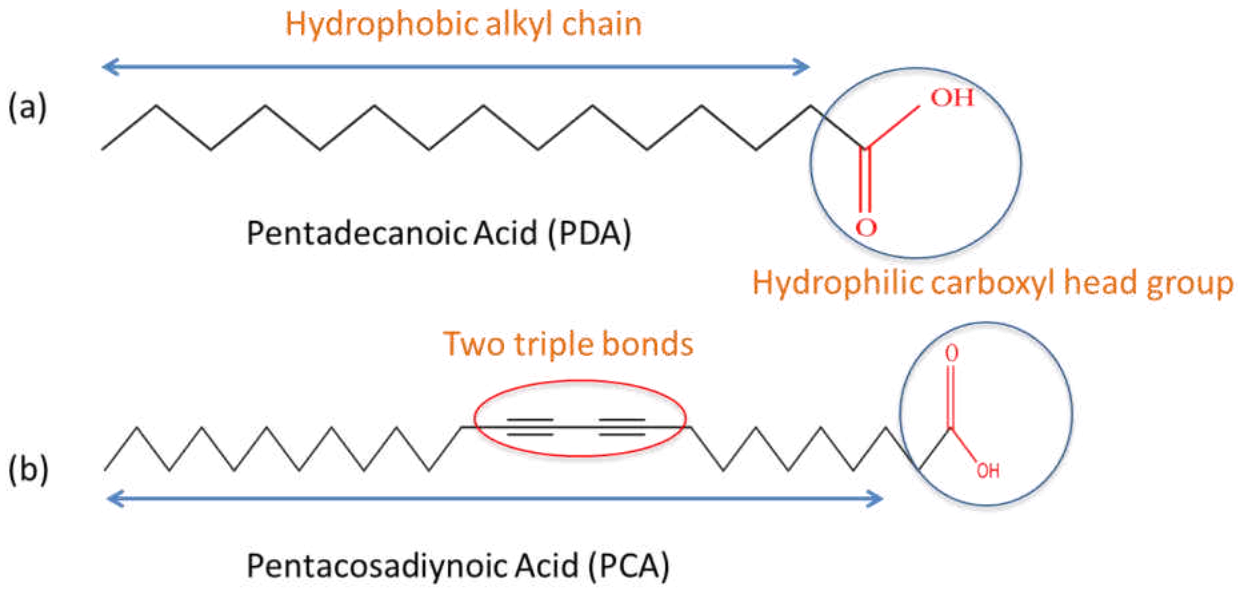

Figure 9 Schematic of molecular structure of (a) PDA and (b) PCA.

H. D. Sikes et al. observed the densely-packed islands and dendritic structure in AFM pictures by transferring PDA monolayers in liquid expanse phase (LE) onto mica substrates[64]. Keith J. Stine and his coworkers found foam structures at the air/water interface of PDA monolayers with BAM in the coexistence phase[65]. In the study by S. Akamatsu et al.[66], fluorescence microscopy pictures also showed the foam structures in the air/water interface in the LE and LC coexistence phase range. And their work showed circular shape LC domains were isolated by large areas of LE phases. They showed the surface pressure increased as the increase of temperature. Shape relaxation of PDA after compression stopped had also been noticed in their work. Inversed boojum[67] was discovered in the LE-LC coexistence phase at the air/water interface by using BAM on the water surface.

PCA is a diacetylene compound (R-C≡C-C≡C-R'), and is well known of its photoreactivity by UV irradiation[68]. With appropriate stimulation (E.X. UV light radiation) in the solid state, diacetylene compounds can polymerize[69, 70]. Linear polymerization of PCA on graphite surface has been shown to have a length ranging from 5 to 300 nm[71].

CHAPTER 2. EXPERIMENTAL

2.1 Pentadecanoic acid (PDA) and 10, 12-Pentacosadiynoic Acid (PCA) Synthesis

Pentadecanoic (PDA) from Sigma was dissolved in chloroform, and 10, 12-Pentacosadiynoic Acid (PCA) from Aldrich was dissolved in toluene before spreading onto the air/water interface in a NIMA Langmuir trough. Water used in our experiments was puritfied by a Millipore Milli-Q system. Surface pressure-area isotherms of PDA monolayers were identical to those reported in literature[21]. Polymerization on PCA was performed with UV (254nm) at the air/water interface before transferred onto a substrate at room temperature (~22℃). The subphase temperature was controlled by a circulating water bath through the base plate of the Langmuir trough.

2.2 Sample Preparation

Glass substrates were cleaned by a solution of 70% H_2SO_4/30% H_2O_2 at 100℃ for 30 min and then rinsed thoroughly with Milli-Q water. Glass substrates were inserted into the water subphase prior to the spreading of PDA/PCA monolayers. After solvent was allowed to evaporate for 15 min, the PDA/PCA monolayers were compressed at a rate of 1 $Å^2$ molecule $^{-1}$ min^{-1} and then transferred onto glass substrates at a constant speed after a preset pressure was reached. The transferred monolayers were stored in a sealed container for no more than a day prior to imaging.

Liquid crystal imaging cells were assembled by using a PDA/PCA monolayer covered glass substrate in the bottom and a cleaned glass slide on top with a 25 μm spacer in between, as shown in figure 10. Liquid crystal 5CB (4'-pentyl-4-cyanobiphenyl) was applied as an optical amplification medium to image the textures in the transferred PDA/PCA monolayer. 5CB was employed into the cells in the isotropic phase and cooled down to room temperature after the cell was fully occupied.

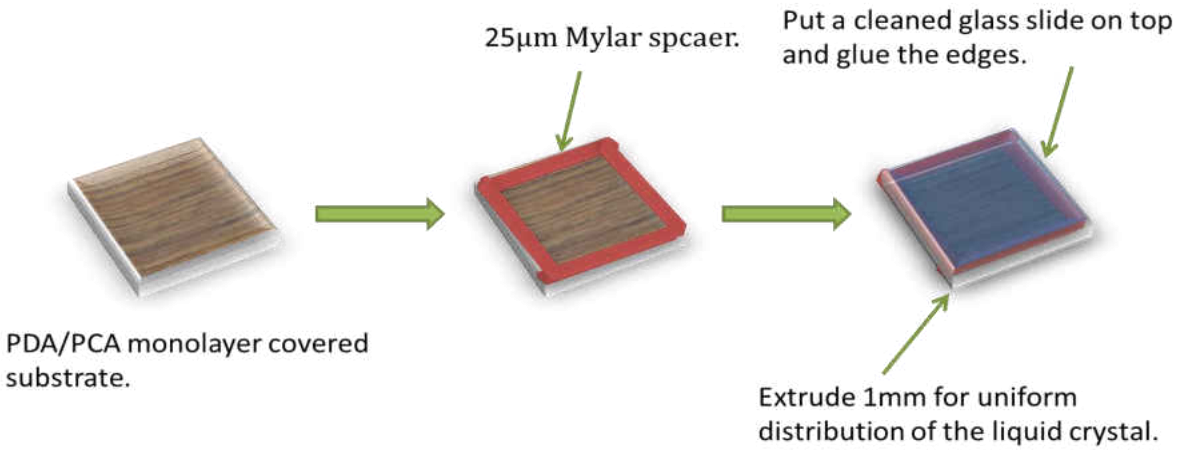

Figure 10 Schematic representation of assembling liquid crystal imaging cells.

2.3 Characterization Tools

2.3.1 Atomic Force Microscope (AFM)

Frictional force images of PDA/PCA monolayers on glass substrates were achieved by using an atomic force microscope (AFM) (Dimension 3100, Vecco Instruments) in contact mode in air at room temperature (~22℃). A silicon nitride cantilever (Nanosensors) with a spring

constant of 0.051 N/m was used. The size of the cantilever tips (radius of curvature) according to the manufacturer was about 15 nm. Typical loading forces were on the order of 1nN.

2.3.2 Optical Microscope

Optical microscope (BX 40 Olympus) was used to visualize the orientation variation of 5CB induced by the PDA/PCA monolayers of the liquid crystals imaging cells. Images were captured by the attached digital camera (Olympus C2020 Zoom) mounted on the microscope.

CHAPTER 3. RESULTS AND DISSCUTION

3.1 Pentadecanoic acid (PDA)

Amphiphilic molecules attract great interest in the biology and chemistry field because of their monolayers at the air/water interface are excellent models for studying the biological processes in cell membranes[4, 72] and the phase transitions in quasi two-dimensional systems[3, 22]. Besides, some technological potential are shown in, such as molecular electronics, biosensors and nonlinear optics after the monolayers are transferred to solid substrates[19].

Monolayers at the air/water interface have one important feature, which is the existence of long-range orientational order[3, 22]. The star[73-75], stripe[76-78] and boojum textures[79-81] represent the long-range organization of the molecular tilt azimuth in which the tilt angle of molecules with respect to the surface normal is fixed by the thermodynamic state, but the tilt azimuth is not. The molecules have the same tilt azimuth director which is parallel to the segment bisector in one segment of the star texture. Figure 11a shows a discrete jump in the tilt azimuth between segments. The tilt azimuth turns continuously in the boojum texture in Figure 11b. The points with the same tilt azimuth are located on a straight line, crossing at a single defect point which is located just outside the domain boundary. The stripe texture has both the discrete jump and continuously feature which is shown in Figure 11c. The director of the tilt azimuth in one stripe turns continuously and jumps at the boundary between each stripe.

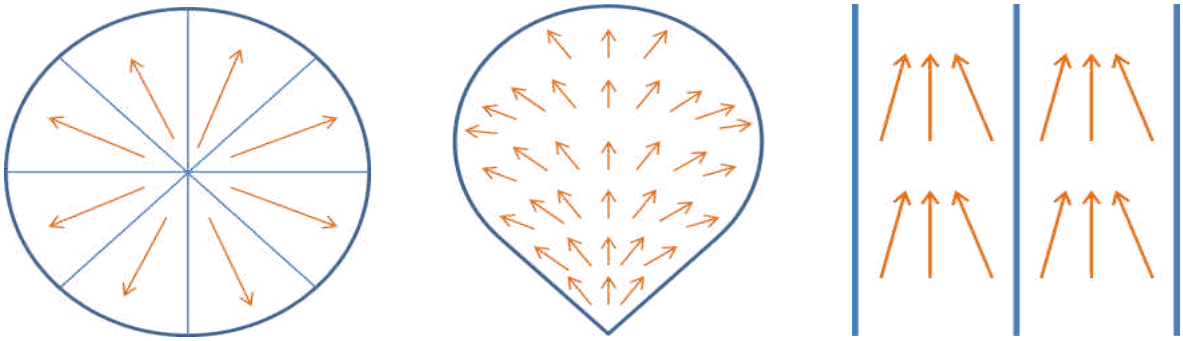

(a) (b) (c)

Figure 11 Schematic of molecular tilt azimuth within (a) star, (b) boojum and (c) stripe textures.

Stripe texture forms in monolayers of pentadecanoic acid (PDA) when compressed to an area of 25−35 $Å^2$/molecule and the liquid expanded (LE) phase is replaced by the liquid condensed (LC) phase when cooled below the triple point, as shown in the work of J. Ruiz-Garcia et al.[76].

In the study of D. K. Schwartz[79], a PDA monolayer with 1 mol % NBD-hexadecylamine at the air/water interface within the liquid expanded (LE) and liquid condensed (LC) coexistence phase in the range of 15−25℃, the LC domains showed the boojum textures under the polarized fluorescence microscope (PFM). The cusp angle of the boojums varies and in related with the radius of the LC domains[79, 80].

3.1.1 Boojum textures of PDA monolayer

The frictional force microscopy (FFM) image of an LE-LC coexistence phase transferred from the air/water interface onto a glass substrate at 18℃ with a dipping speed of 0.2 mm/min

using the Langmuir-Blodgett (LB) technique (Figure 12a). It was taken from the left-to-right scan at room temperature (22℃). The boojums are successfully preserved on the glass substrate under these conditions during the LB transfer process, although the uniform LE phase breaks up into small islands which leads to the exposure of the glass substrate surface (bright region). In each LC domain boundary, the cusp is noticeable. Due to the reduce friction force in the boojums domain compare to the glass substrate surface, because the boojums are softer than the glass, the boojums are dark in the FFM image. Figure 12b shows when the LE-LC coexistence phase transfer at the air/water interface is performed at 12℃, the uniform LE phase is found out to be preserved on the glass substrate and shows a uniform grey scale. Small bright dots appear in the gray LE phase around the dark LC domains when the LE-LC coexistence phase is transferred onto glass substrates at 8℃ (Figure 12c). The bright dots have higher friction than the gray LE phase (middle friction) and dark LC domains (low friction). The bright dots appear during the cooling of the LE-LC coexistence phase representing the gas (G) bubbles are formed[76], which means a G-LE-LC coexistence phase is successfully preserved after the transfer. At the loading of 1nN, the relative friction force of G, LE, LC phases is 7:4:1.

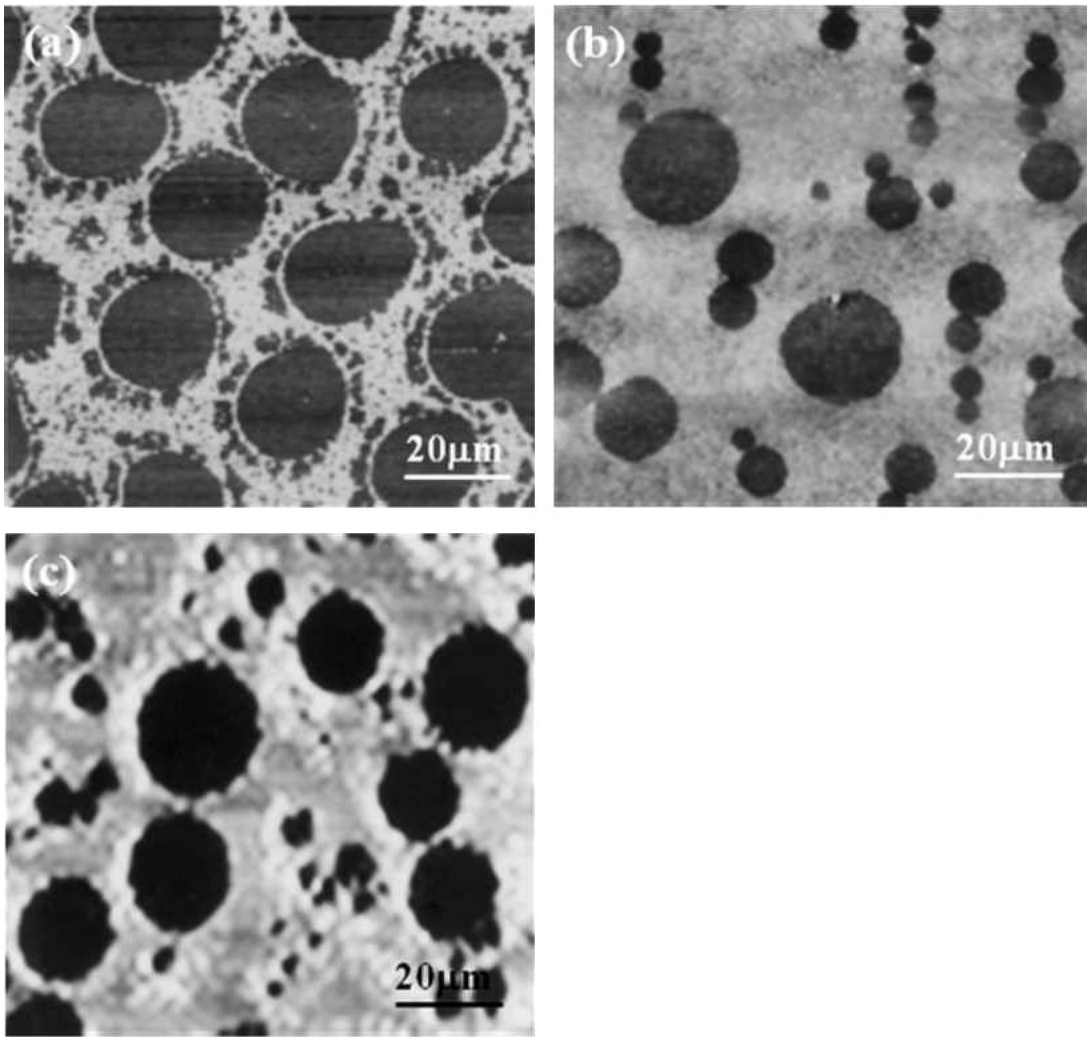

Figure 12 Frictional force images of an LE-LC coexistence phase from the air/water interface transferred onto glass substrates at a dipping speed of 0.2 mm/min at (a) 18℃, (b) 12℃, and (c) 8℃. The images were taken from the left-to-right scan in air at 22℃.

In Figure 12a, there are clearly no evident shows the boojum shape is distorted when transferred at a dipping speed of 0.2 mm/min. But after transferred whether the continuous variation of tilt azimuth within the boojums is preserved on the glass substrate is another

interesting issue. The ability to dissolve the discrete jump of the tilt azimuth between segments in the star textures has been shown by FFM[22, 82-84].

Figure 13a shows a high resolution image of FFM measurements of an individual boojum, in which the boojum that is aligned with the scan direction appears to be homogeneous in friction. In Figure 13a, it looks like no detectable changes in friction are noticeable with the continuous variation of molecular tilt azimuth with respect to the scan direction. But inhomogeneous frictions are observed when the boojums are aligned by ~45° to the scan direction, which are shown in Figure 3b and 3c. We expect there is a discrete jump in the tilt azimuth with respect to the scan direction along the longest radius of the boojums base on the variation of molecular tilt azimuth in the boojum texture (Figure 13b). As shown in Figure 13b and 13c, when the scan direction is opposite the scan direction, the friction is high (bright region); when the scan direction is in the tilt direction, the friction is low (dark region). No variation in friction is observed within both regions. In addition, the boundary between the two regions is curved, which implies the dipping process very likely affects the continuous tilt azimuth variation in the boojums.

We find the transferred boojums are aligning along the dipping direction when the dipping speed increases to 2 mm/min, as shown in Figure 14. It has been shown LB transfer causes flow in monolayers[85, 86]. In Figure 14 all the cusps of the aligned boojums point in the same direction, which shows the high dipping speed transfer very likely induces the alignment of boojums. Additionally, some of the boojums start to break up along their radial direction, while most of them are elongated along the dipping direction at the higher dipping speed.

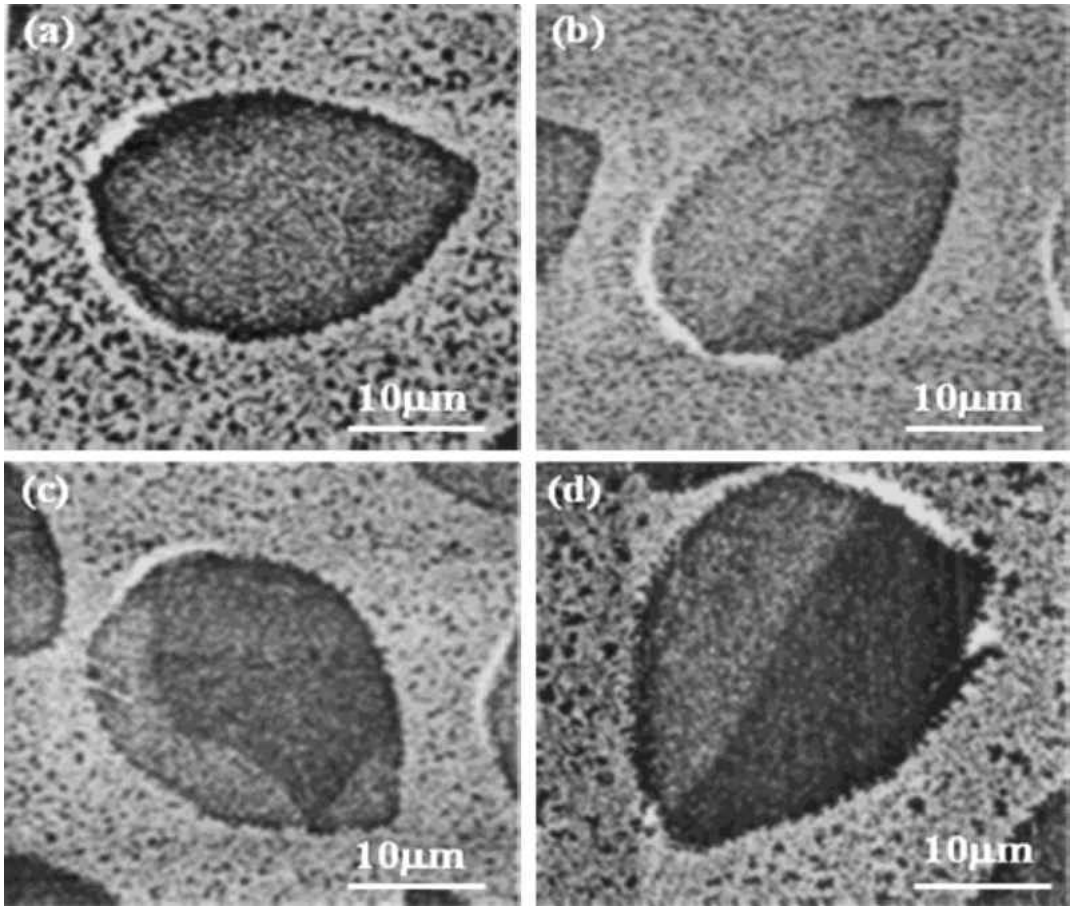

Figure 13 AFM images of different orientations of boojums on glass substrates with respect to the scan direction. These images were taken in air at 22℃; the scan direction was from left to right. The transferred speed of boojums onto glass substrates was 0.2 mm/min at a temperature of 18℃.

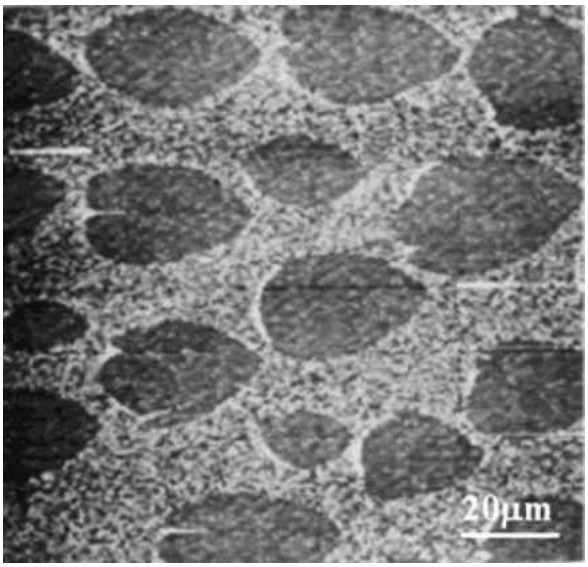

Figure 14 Frictional force image of a transferred monolayer on glass substrate from an LC-LE coexistence phase at the air/water interface at 15℃ with a speed of 2 mm/min. The image was taken from the left-to-right scan in the air at 22℃.

3.1.2 Stripe textures of PDA monolayer

The G-LE-LC triple point of PDA monolayers was determined to be 17℃ at the air/water interface[87]. The molecular area of the LE phase is 43 $Å^2$/molecule and 2100 $Å^2$/molecule for the GF phase at the triple point. When compressed to a molecular area of 25−35 $Å^2$/molecule and cooled below the triple point, the stripe textures which had a width vary from 5μm to 80μm could be formed in a PDA monolayer[76, 77]. In our study, using the LB technique, PDA monolayers were transferred onto glass substrates at 8℃ at a dipping speed of 0.2 mm/min. Friction force images taken in air at room temperature (~22℃) of the stripe texture on glass substrates are shown in Figure 5. The width of stripes is ~20μm measured by frictional force images, and is consistent with the study of PDA stripes width range at the air/water interface by fluorescence microscopy[77].

Frictional force image (Figure 15a) shows a continuous variation across each stripe for the stripes perpendicular to the scan direction. The topographical image taken simultaneously shows no feature. For molecules have the same tilt angel with respect to the surface normal in the same stripe, there is no variation in the heigh profile. If there is friction variation within one stripe, it is reasonable to assume the molecular tilt azimuth in the stripe is varied. However, the precise relationship between the friction and the tilt azimuth is hard to define base on the data we generate from the FFM measurements. The presence of stripes in the transferred monolayer, the uniformity of height, and the variation of the frictional force all support our view that the stripe texture survives the transfer to glass substrates at the low dipping speed. However, it does not necessary mean all the transferred PDA stripes are perfect.

Figure 15b shows defects of PDA stripes on a glass substrate imaged by FFM are characteried by the discontinuous variation in frictional force. The spiral pattern found by FFM on glass susbtrates, which is shown in Figure 15c, is formed by the organization of stripes at the air/water interface around a point defect[76]. Due to the limit of the maximum scan range (100μm) of the friction force microscope we use, it is impossible to image a whole spiral. The spiral pattern from Figure 5c, however, shows the friction force of the stripes exhibit near symmetrical variations across their width. The transfer of stripe textures was carried out at 8℃ from the air/water interface and the friction force images were taken at 22℃ in air, which suggests the continuous variation of the molecular tilt azimuth within the stripes is frozen on glass substrates. The variations in friction across the width within the stripes disappear when we increase the dipping speed to 2 mm/min, which means the orientation of the PDA molecules within the stripes are reorganized by the higher dipping speed.

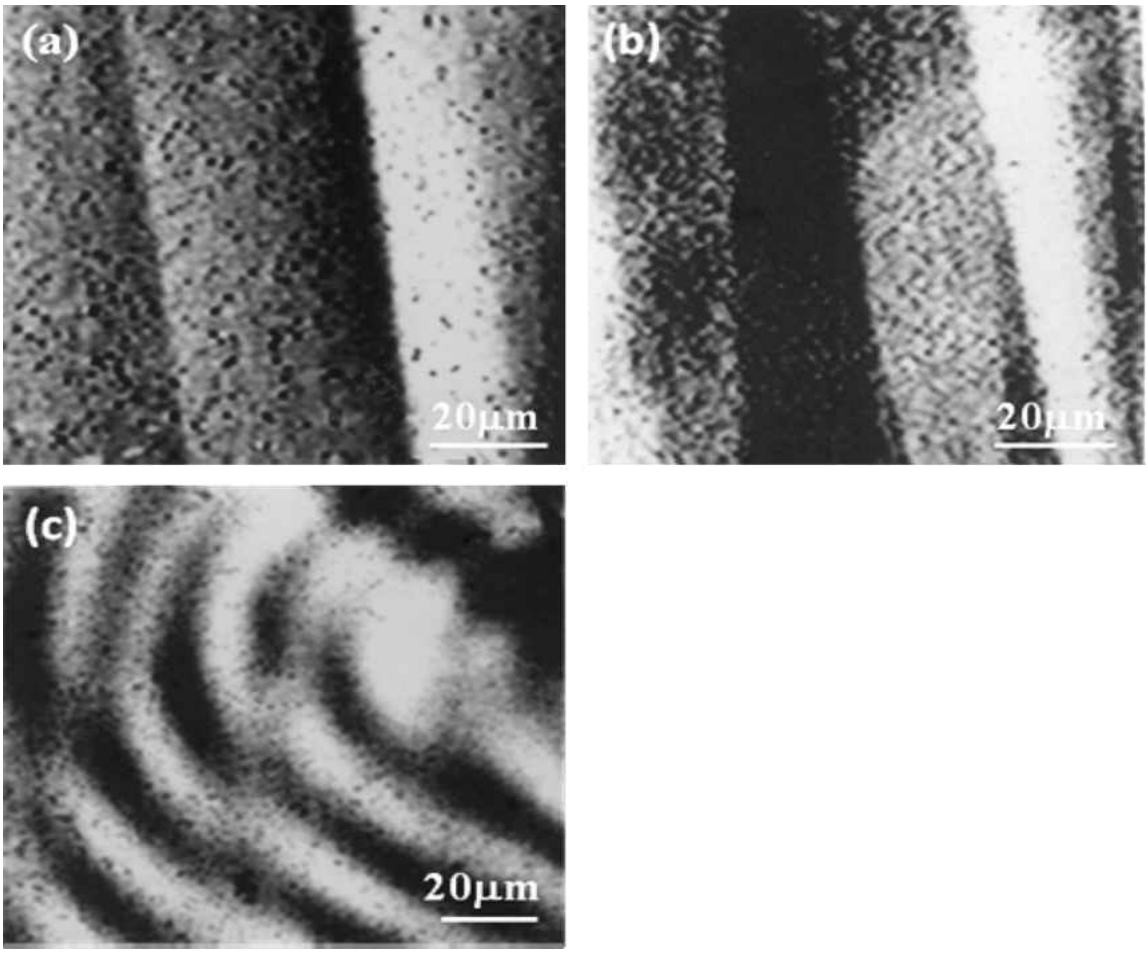

Figure 15 Frictional force images of stripe textures transferred on glass substrates at 8℃ with a speed of 0.2 mm/min from the air/water interface. The images were taken from the left-to-right scan in air at 22℃.

Figure 16 shows the schematic geometry of the liquid crystal (5CB) imaging cell of a PDA monolayer. Light propagates from below the imaging cell and passes through the polarizer, then the liquid crystal which rotates its plane of polarization, in the end out through the analyzer. The director represents the local orientation of the molecules and determines the optical properties of the liquid crystal. The images of the optical textures are captured by using a polarizing microscope with a hot stage.

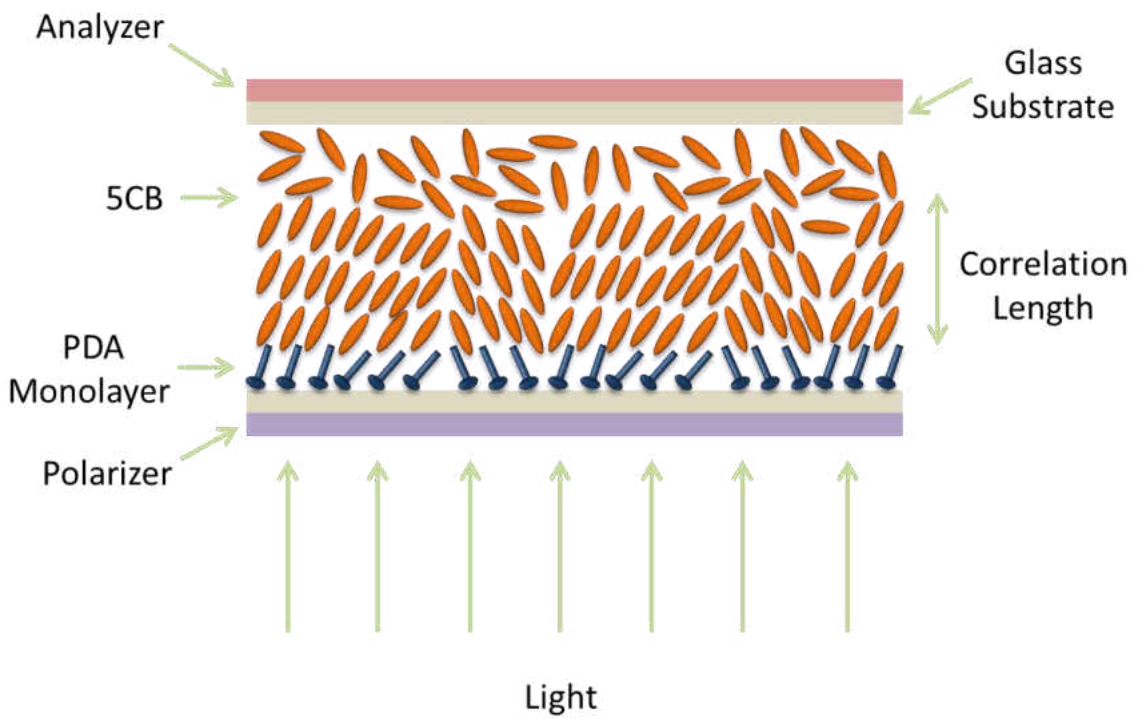

Figure 16 Schematic geometry of liquid crystal (5CB) imaging cell of a PDA monolayer. A tilted monolayer is deposited on the bottom glass slide. 5CB is employed above the tilted layer.

The application of liquid crystals has been explored as in imaging self-assembled organic and biological systems[60, 63, 88] and detecting biological binding events[56, 60, 89]. In our study, we use optical amplification of liquid crystals (5CB) to further image the frozen organization of the tilt azimuth within the transferred stripes on glass substrates. Liquid crystal (5CB) image of stripes (Figure 17a) was taken by a polarizing optical microscope under crossed polarizers at the nematic phase of 5CB. The stripe textures in the liquid crystal images closely resemble what has been shown by BAM on the water surface[76, 78]. Figure 17b shows the plots of transmitted intensity across the stripes, closely resembling the fluorescence intensity profile across PDA

stripes with 1 mol % NBD-hexadecylamine measured at the air/water interface[78]. The transmitted intensity reaches maximum near the center while the minimum appears at both edges. The tilt azimuth direction of the 5CB varies continuously across the stripes induces the variation of the transmitted intensity. The transmitted intensity also varied when the sample was rotated between crossed polarizers.

When 5CB is heated to its isotropic phase, the stripes shown in Figure 6a disappear and reappear while 5CB is cooled down to its nematic phase, which suggests the azimuthal order of 5CB molecules is induced by the transferred stripes. People have been using LB technique to transfer monolayers of amphiphilic molecules on glass substrates to align liquid crystals for a long time[90-92]. The penetration of liquid crystal molecules in the transferred monolayers was suggested to the mechanism to induce a homeotropic alignment. The 5CB molecules penetrate into the stripes and align parallel along the tilted PDA molecules via intermolecular interactions, which lead to the continuously azimuthal variation of 5CB across the PDA stripes.

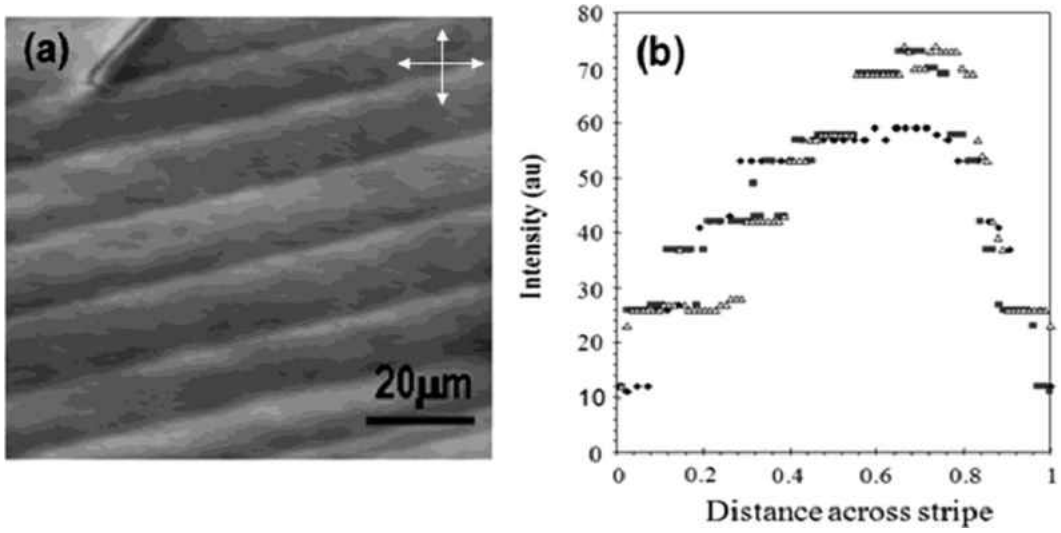

Figure 17 (a) Liquid crystal (5CB) image of stripe textures in a transferred monolayer. The image was taken with an optical microscope under crossed polarizers at 22℃. Arrows indicate the directions of polarizer and analyzer. (b) Plots of the intensity of transmitted light as a function of a fractional distance across the stripes. The intensity was measured by image analysis with *MATLAB* software.

3.2 10, 12-Pentacosadiynoic Acid (PCA)

10, 12-Pentacosadiynoic acid (PCA) at the air/water interface has been widely studied[93-96]. X-ray diffraction study on polymerized PCA by UV light irradiation with two different subphases of $CdCl_2$ and $TbCl_3$ showed the molecular packing of the monolayer was influenced and in turn influenced the polymerization[93]. Brewster angle microscopy images showed domains of PCA monolayer formed immediately after spreading and packed up as surface pressure increased[94]. The condition to trigger polymerization and the possible ways to polymerize of PCA were discussed in the study of K. Ogawa, in which evidence was shown that the sensitivity of PCA polymerization was affected by the molecular density in PCA LB film[95]. The phase

diagram of PCA had been studied by detailed isotherm measurements[97]. What also should be noted is PCA monolayers are unstable and collapses on pure water[97], while they can be stabilized by spreading on a subphase[98]. The length of extended PCA molecule is about 3.1~3.2 nm[99-100].

Figure 18 shows the surface pressure/area isotherm of the PCA monolayer on water subphase obtained by continuous compression. The isotherm we obtained is similar to former studies[97-98, 100-101]. From the results of our experiment, different from PDA, the pressure-area isotherm reflects the PCA molecule arrangements from single layer to multilayer. The first steep increase of surface pressure indicates the formation of a monolayer.

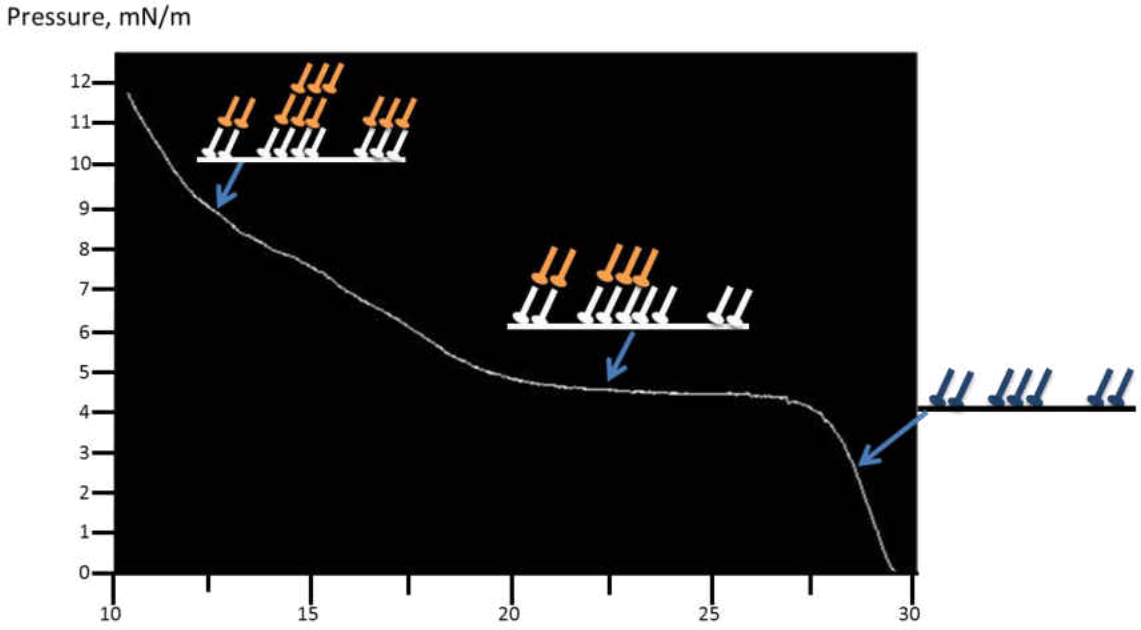

Figure 18 Surface pressure/area isotherm of PCA monolayer on water subphase.

3.2.1 Topographic AFM images of PCA stripes on glass substrates

We used the LB technique to transfer PCA monolayers with stripe textures on glass substrates at the LC phase with a dipping speed of 0.2 mm/min at 18℃. Figure 19 shows an

atomic force microscope (AFM) image of PCA stripe textures transferred on a glass substrate. Transferred of the film performed at a pressure of 3.6 mN/m and a molecular area of 27.8 $Å^2$. The image was taken in air at room temperature (22℃). PCA stripes pattern is transferred onto glass substrates from the figure. The topographical image shows the height variance across the stripes along the scan direction, which indicates the tilt angle of PCA molecules changes in different stripes. Due to the lack of friction force profile, we cannot conclude whether the tilt azimuth is the same along a single stripe. As the transferred pressure increases to 5.8 mN/m at which PCA has 18.2 $Å^2$/molecule (Figure 20), AFM image shows stripes with different directions are transferred onto the glass substrate. The overlap of different stripes is also shown in the image. PCA molecule has a polar surface area of 26.3 $Å^2$, which means the arrangement of molecules at the air/water interface is not able to maintain monolayer and induce formation of a multilayer. The structure of PCA molecule implies the arrangement of molecules will be tilted yet the tilt angle and tilt azimuth is not fixed. Therefore the molecules arrangement in the multilayer has a high uncertainty.

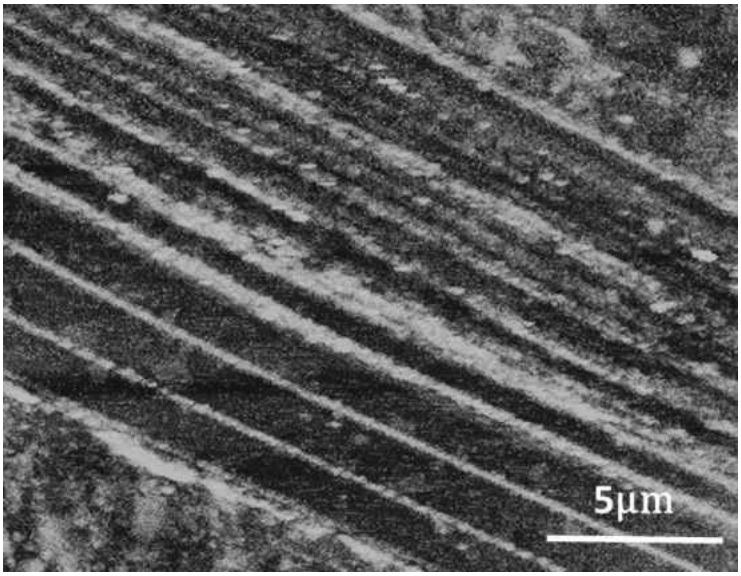

Figure 19 Atomic force microscope image of stripe textures transferred from PCA monolayers at the 3.6 mN/m on glass substrates with a speed of 0.2 mm/min at 18℃.

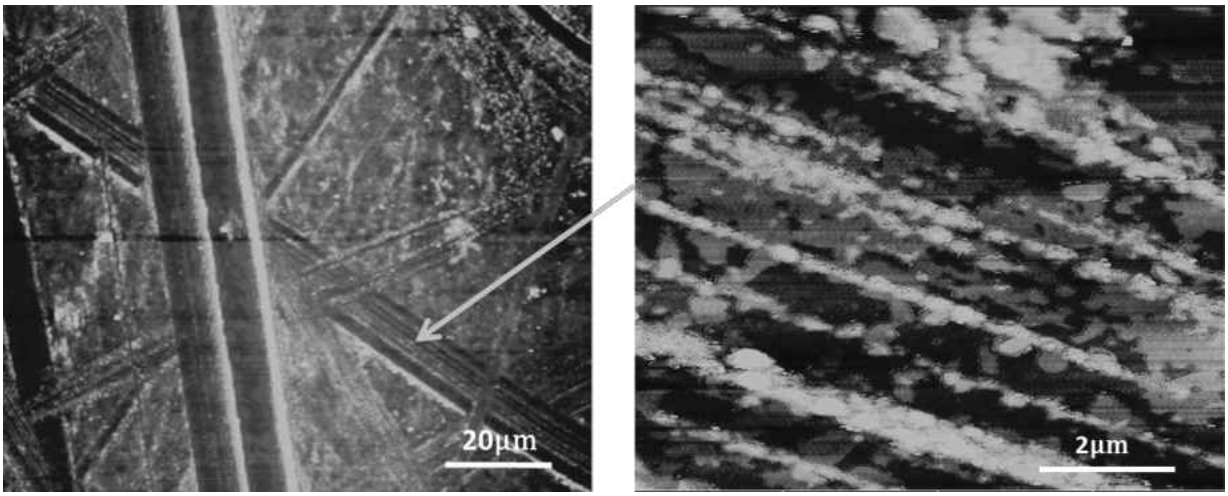

Figure 20 Atomic force microscope image of stripe textures transferred from PCA monolayers at the 5.8 mN/m on glass substrates with a speed of 0.2 mm/min at 18℃.

3.2.2 Alignment of 5CB on PCA stripe textures on glass substrates

First observation of the imaging cell after filled with 5CB was obviously that the nematic phase of 5CB wetted the PCA monolayer covered glass substrate completely. Figure 21 shows liquid crystal (5CB) images of the stripe textures transferred at the air/water interface at pressure 5.8 mN/m. The images were taken by a polarizing optical microscope under crossed polarizers when 5CB is in its nematic phase. As shown in Figure 21, the stripes were lighted up by 5CB and the brightness changed as the sample rotated. In Figure 21 (a) and 21 (d), the light intensity through the stripes achieved the maximum when the sample was arranged parallel or perpendicular to the polarizer; light intensity decreased in the angle range of 0° to 45° with respect to the polarizer (Figure 21 b), and had its minimum at the 45° (Figure 21 c), then increased again in the range of 45° to 90°. From these results, we concluded the PCA stripes induced the nematic 5CB azimuthal orientation uniformly in a direction about 45° to the stripes axis. The light intensity change had no regular pattern in the LE phase area in Figure 21, indicating the nematic 5CB molecules were orientated with a large angle with respect to the surface normal.

During the compression, the reduction in molecular areas meaning the increase of packing densities at the air/water interface. While being transferred onto the substrate, the hydrophilic head group of PCA interacted with the hydrophilic glass substrate and stick on it, while the hydrophobic tail stood up. Due to the hydrophobic feature of nematic 5CB, within the stripes 5CB interacted with the hydrophobic tail of PCA and tilted by an angle with respect to the surface normal. The penetration of 5CB molecules in lipid monolayers[91, 92] can also be used for explaining the 5CB interaction with PCA monolayers. Due to short range interaction[102] and close hydrophobicity, partially of the first layer 5CB molecules may penetrate into the PCA

monolayers while the others titled and acquired a polarized dipolar surface layer[103]. The long range orientation of nematic 5CB later on leads the interface-induced orientation to the bulk phase and adopts the orientation of the PCA monolayer. Therefore, we conclude that the orientation of 5CB shown in Figure 21 reflects the variation of packing densities leaded PCA stripe pattern.

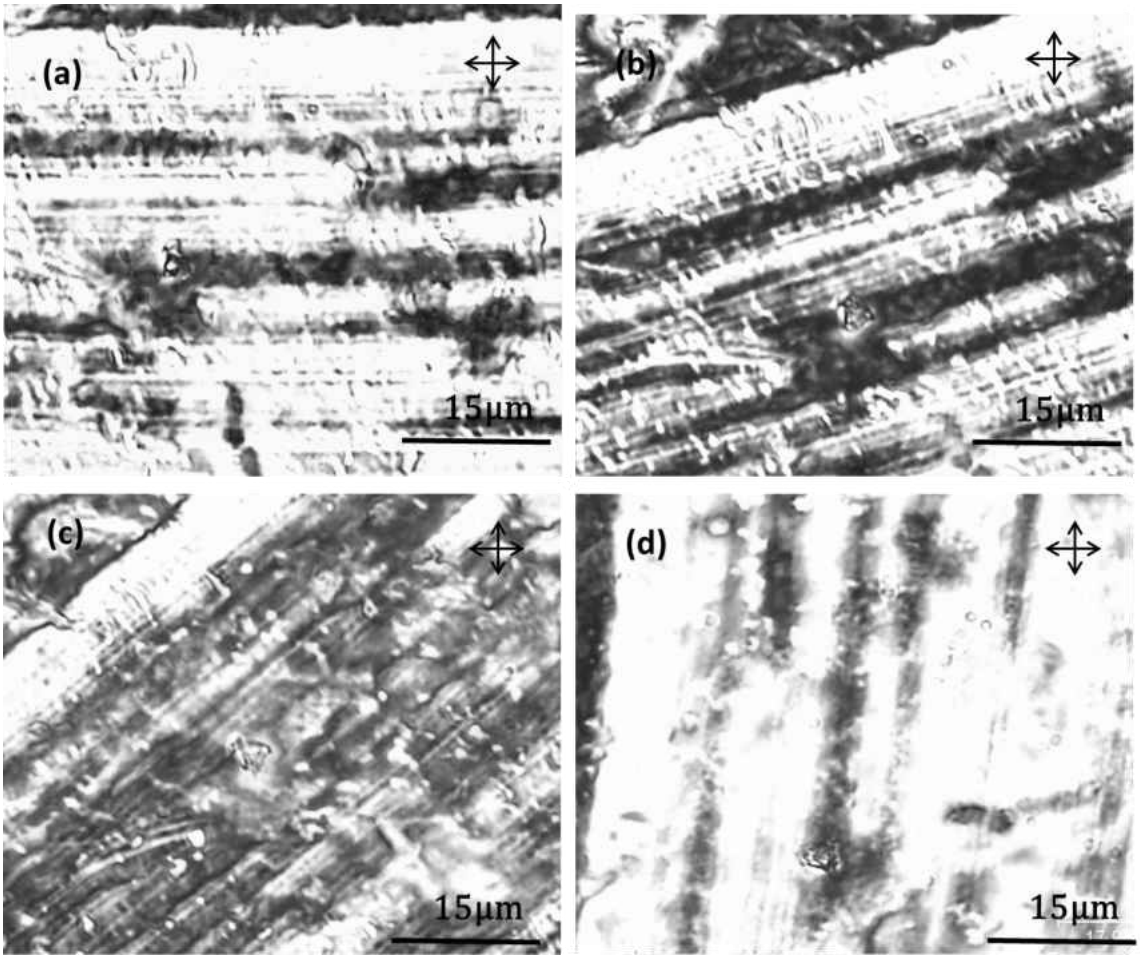

Figure 21 Liquid crystal (5CB) images of stripe textures in a transferred monolayer. Transferred at a pressure of 5.8 mN/m with dipping speed 0.2 mm/min at 18℃. Stripes were (a) parallel, (b) 20°, (c) 45°, and (d) perpendicular to the polarizer. The images were taken with

an optical microscope under crossed polarizers at 22℃. Arrows indicate the directions of polarizer and analyzer.

As heated up to the isotropic state of 5CB at 36℃, the stripes pattern disappeared under polarized microscope as shown in Figure 22 (d). Figure 22 (a) shows the image of the alignment of 5CB on PCA stripe textures at 22℃. As temperature increase, the thermo motion of liquid crystal molecules increase and affects the molecular interaction in the bulk phase as well as at the interface as shown in Figure 22 (b, c). When cooled down to its nematic phase at 22℃, the PCA stripe textures reappear, suggesting the alignment of 5CB molecules is induced by the PCA stripes.

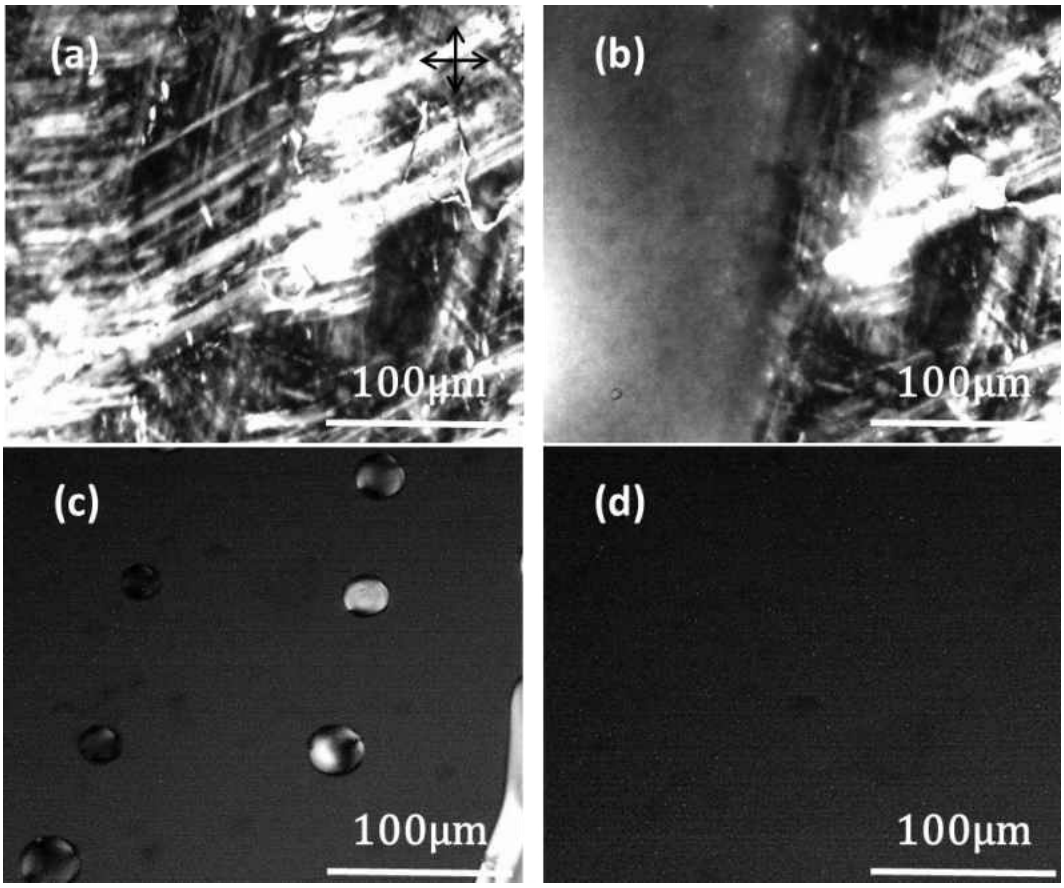

Figure 22 Liquid crystal (5CB) images of stripe textures in a transferred monolayer. Transferred at a pressure of 5.8 mN/m with dipping speed 0.2 mm/min at 18℃. The images were taken at temperature (a) 22℃, (b) 30℃, (c) 34℃, and (d) 36℃ with an optical microscope under crossed polarizers. Arrows indicate the directions of polarizer and analyzer.

3.2.3 Alignment of 8CB on PCA stripe textures on glass substrates

8CB has been well studied[45, 104-105], which is smectic-A liquid crystal at room temperature and the nematic phase transition temperature is 33.3℃[106]. The smectic-A 8CB has a strong dipole to dipole interaction along the axis of the molecules[107] which leads to a bilayer configuration. Figure 23 shows the liquid crystal (8CB) image of PCA stripe textures in a

transferred monolayer at pressure 6 mN/m. The image was taken with an optical microscope under crossed polarizers at 23℃. The 8CB was employed at the isotropic state into the imaging cell to prevent flow-induced anchoring and later on cooled down to room temperature. In Figure 23, the 8CB molecules were presented in pattern representing the PCA stripes. The brightness changed as the sample rotated with respect to the surface normal. 8CB is more rigid and hydrophobic than 5CB[108]. The steric interaction is an important factor to the tilt angle of the molecules near the interface[109]. The polar interactions between 8CB and the monolayer at the interface increase with increasing density of alkyl chains[110-112]. The molecule to molecular forces of 8CB and PCA at the interface are very strong due to the close hydrophobicity and large alkyl tail−8CB interactions cause by high packing density of PCA at the LC phase. The bulk ordering of 8CB is dominated by a combination of the intermolecular dipole to dipole interactions and the molecular forces at the interface between 8CB and PCA. Therefore based on Figure 23 that the 8CB represented the ordering of the PCA stripes pattern, the PCA alkyl tail−8CB interactions dominated the bulk ordering of the liquid crystal.

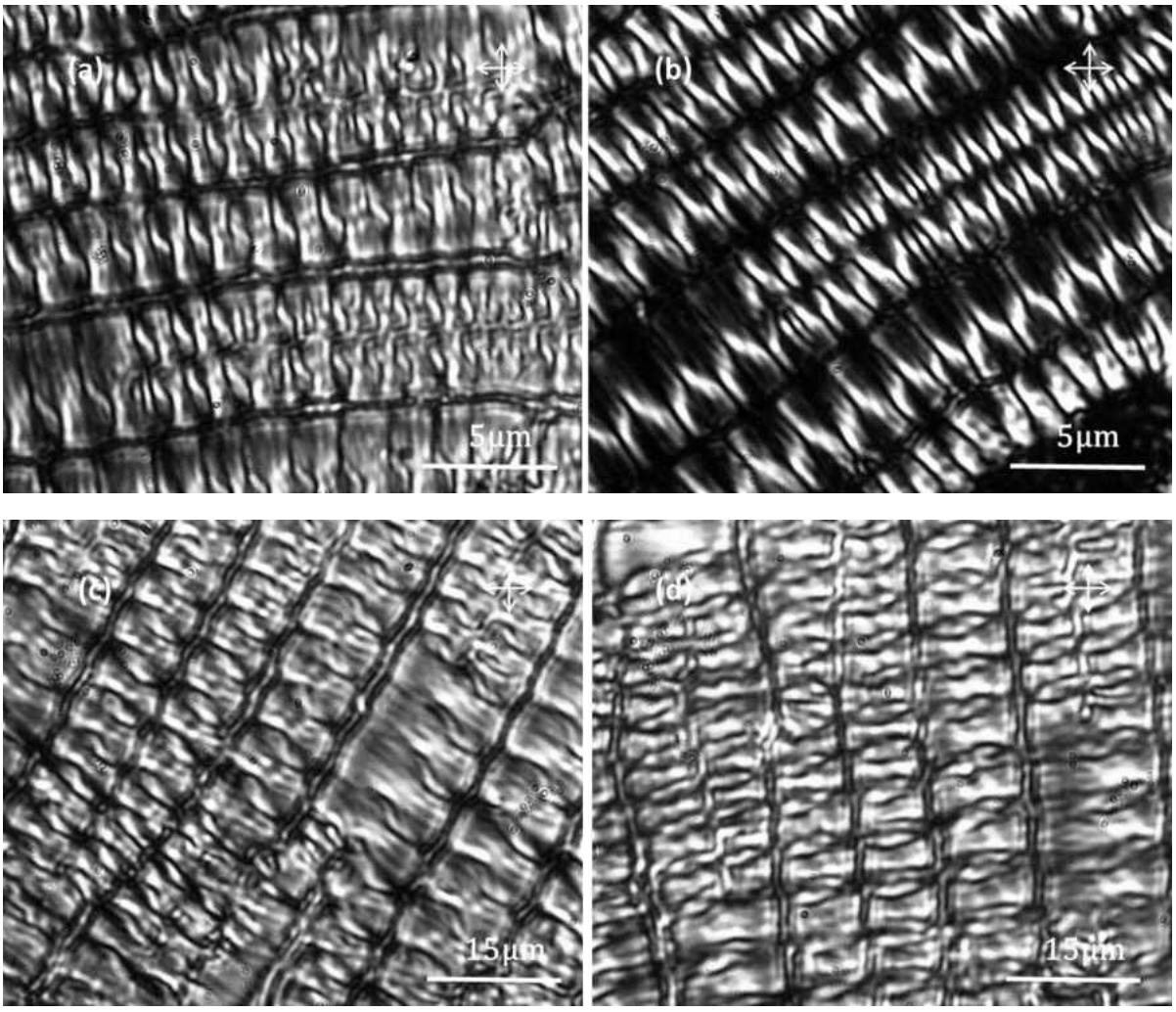

Figure 23 Liquid crystal (8CB) image of PCA stripe textures in a transferred monolayer at pressure 6 mN/m. The image was taken with an optical microscope under crossed polarizers at 23℃. Arrows indicate the directions of polarizer and analyzer.

Figure 7 shows the Liquid crystal (8CB) images of polymerized stripe textures in a transferred monolayer at pressure 6 mN/m. The images were taken with an optical microscope under crossed polarizers at 37℃ which 8CB is in the nematic phase. 8CB is less rigid and lower

viscosity in the nematic phase compared to the smectic-A phase. The intermolecular dipole to dipole interactions reduce, the 8CB molecules continuously orientated along the PCA stripes.

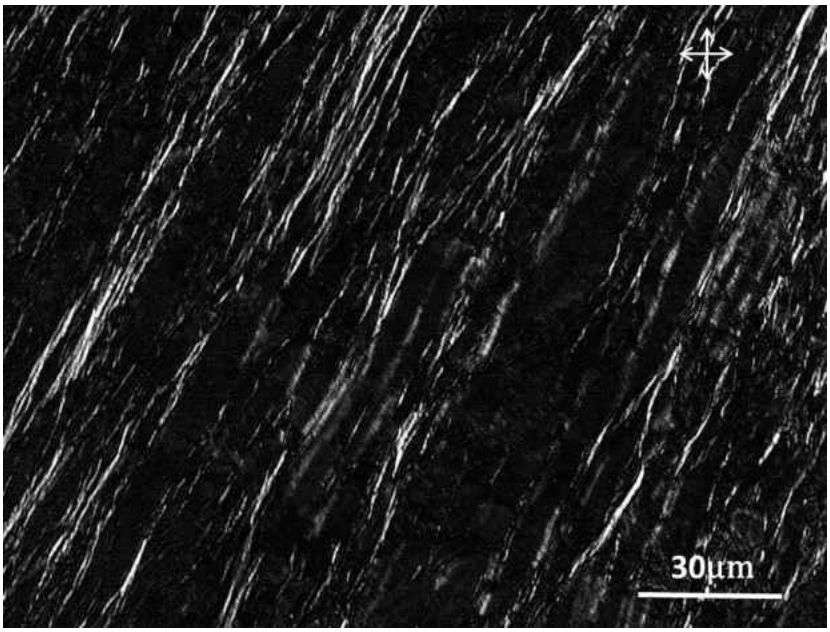

Figure 24 Liquid crystal (8CB) images of PCA stripe textures in a transferred monolayer at pressure 6 mN/m. The images were taken with an optical microscope under crossed polarizers at 37℃. Arrows indicate the directions of polarizer and analyzer.

CHAPTER 4. CONCLUSION

AFM and polarized microscope are successfully used to study the transferred PDA and PCA monolayers. We report the both PDA and PCA monolayer textures are finely remained after transferred to solid substrates.

We demonstrate PDA monolayers at the air/water interface can be transferred onto glass substrates at low dipping speeds without altering their long-range tilt order. The stripe and boojum textures of PDA monolayers with continuous variation of the molecular tilt azimuth formed at the air/water interface at temperatures lower than room temperature are also successfully preserved after transferred. By carrying out frictional force microscopy measurements at room temperature, we discover the continuous variation of the molecular tilt azimuth in stripe and boojum textures is frozen on glass substrates. The transferred stripe textures can induce a continuously azimuthal variation of 5CB.

We show that the stripe textures of PCA monolayers with regular variations of molecular packing densities at the air/water interface can be transferred onto glass substrates without changing the packing densities. Atomic force microscopy confirms the packing densities variation successfully preserved in the transferred PCA monolayers on glass substrates. The packing densities change in PCA monolayers can induce ordering of nematic 5CB and smetic-A/nematic 8CB. Due to the long-range orientation correlation of nematic 5CB and smectic-A/nematic 8CB, the stripe textures of PCA monolayers can be observed by an optical microscope after liquid crystal optical amplification within the imaging cell. Further study of the ordering induced by PCA monolayers of smectic-A 8CB will open up the possibility to be turned into a unique biosensor.

REFERENCES

1 G. Roberts, *Langmuir-Blodgett Flms* **1990.**

2 P. Martin, M. Szablewski, *Langmuir-Blodgett Troughs* **2001.**

3 V.M. Kaganer, H. Möhwald, P. Dutta, *Rev. of Mod. Phy*. **1999**, 71, 779.

4 H. M. McConnell, Vrljic, *Annu. Rev. Biophys. Biomol. Struct*. **2003**, *32*, 469.

5 G. Baneyx, V. Vogel, *Proc. Natl. Acad. Sci. USA* **1999**, *96*, Art. No. 12518.

6 D. Gidalevitz, Y. Ishitsuka, A. S. Muresan, O. Konovalov, A. J. Waring, R. I. Lehrer, K. Y. C. Lee, *Proc. Natl. Acad. Sci. USA.* **2003**, *100,* 6302.

7 G. H. Wu, J. Majewdski, C. Ege, K. Kjaer, M. J. Weygand, K. Y. C. Lee, *Phys. Rev. Lett.* **2004,** *93,* Art. No. 028101.

8 C. Alonso, T. Alig, J. Yoon, F. Bringezu, H. Warriner, J. A. Zasadzinski, *Biophys. J.* **2004**, *87*, 4188.

9 J. Strzalka, B. R. Gibney, S. Satija, J. K. Blasie, *Phys. Rev. E.* **2004**, *70*, 061905.

10 F. Hoffmann, K. J. Stine, H. Huhnerfuss, *J. Phys. Chem. B.* **2005**, *109*, 240.

11 J. Ignes-Mullol. D. K. Schwartz, *Nature* **2001**, *410*, 348.

12 G. B. Bantchev, D. K. Schwartz, *Langmuir* **2003**, 19, 2673.

13 J. J. Lauridsen, M. Twardos, M. Dennin, *Phys. Rev. Lett.* **2002**, *89*, Art. No. 098303.

14 P. Cicuta, E. J. Stancik, G. G. Fuller, *Phys. Rev. Lett.* **2003**, *90*, Art. No. 236101.

15 E. M. Freer, K. S. Yim, G. G. Fuller, C. J. Radke, *J. Phys. Chem. B.* **2004***, 108*, 3835.

16 C. Alonso, J. A. Zasadzinski, *Phys. Rev. E* **2004**, *69*, Art. No. 021602.

17 J. M. Lopez, M. J. Vogel, A. H. Hirsa, *Phys. Rev. E* **2004**, *70*, Art. No. 056308.

18 E. Hatta, T. M. Fischer, *J. Phys. Chem. B* **2005,** *109*, 2801.

19 A. Ulman, *An introduction to Ultrathin Organic Films: From Langmuir-Blodgett to Self-Assembly* **1991.**

20 K. NØrgaard, T. BjØrnholm, *Chem. Commun.* **2005,** 1812.

21 B. G. Moore, C. M. Knobler, *J. Phys. Chem.* **1990**, *94*, 4588.

22 V. M. Kaganer, I. R. Peterson, R. M. Kenn, M. C. Shih, M. Durbin, P. *J.* Dutta, *Chem. Phys.* **1995**, *102,* 9412.

23 S. Hénon, J. Meunier, *Rev.Sci. Instrum.* **1991,** *62*, 936. D. Hönig, D. Möbius, *J. Phys. Chem.* **1991**, *97*, 4590.

24 S. Riviére, S. Hénon. Meunier, D. K. Schwartz, M. W. Tsao, C. M. Knobler, *J. Chem. Phys.* **1994,** *101*, 10045.

25 M. Hossain, T. Suzuki, T. Kato, *Langmuir* **2000**, *16*, 9109.

26 X. Chen, S. Wiehle, L. Chi, C. Mu, R. Rudert, D. Vollhardt, H. Fuchs, G. Haufe, *Langmuir* **2005**, *21*, 3376.

27 U. Gehlert, G. Wridemann, D. Vollhardt, *J. Colloid Interface Sci.* **1995**, *174,* 392. G. Brezesinski, E. Scalas, B. Struth, H. Möhwald, F. Bringezu, U. Gehlert, G. Weidemann, D. Vollhardt, *J. Phys. Chem.* **1995**, *99*, 8758. G. Weidemann, D. Vollhardt, *Langmuir* **1996**, *12*, 5114.

28 J. Crusats, R. Albalat, J. Claret, J. Ignés-Mullol, F. Sagués, *Langmuir* **2004**, *20*, 8668.

29 J. Ruiz-Garcia, X. Qiu, M. W. Tsao, G. Marshall, C. M. Knobler, G. A. Overbeck, D. Möbius, *J. Phys. Chem.* **1993**, *97,* 6955.

30 E. Hatta, Th. M. Fischer, *Langmuir* **2002**, *18*, 6201.

31 D. K. Schwartz, M. W. Tsao, C. M. Knobler, *J. Chem. Phys.* **1994**, *101*, 8258.

32 J. V. Selinger, Z. G. Wang, R. F. Bruinsma, C. M. Knobler, *Phys. Rev. Lett.* **1993**, *70*, 1139.

33 T. M. Fischer, R. F. Bruinsma, C. M. Knobler, *Phys. Rev. E.* **1994,** *50*, 413.

34 G. Binning, C. F. Quate, C. Gerber, *Phys. Rev. Lett*. **1986**, 56, 930.

35 P. G. deGennes, *The physics of Liquid Crystals,* **1974.**

36 B. Jerome, *Rep. Prog. Phys.* **1991**, *54*, 391.

37 F. Reinitzer, *Monatsch, Chem*. **1888**, *9*, 421.

38 O. Lehmann, Z. Physikal, *Chem*. **1889**, *4*, 462.

39 S. Chandrasekhar, B.K. Sadashiva, K.A. Suresh, *Pramana,* **1977**, *9*, 471.

40 J. Billard, J.C. Dubois, H.T. Nguyen, A. Zann, *NouV. J. Chim.* **1978**, *2*, 535.

41 D. Demus, H. Demus, H. Zaschke, *Flüssige Kristalle in Tabellen*, *Deutscher Verl. F. Grundstoffindustrie* **1974.**

42 D. Demus, H. Zaschke, *Flüssige Kristalle in Tabellen II, Deutscher Verl. F. Grundstoffindustrie* **1984.**

43 G. Friedel, *Ann. Physique*, **1922**, *18*, 273.

44 V.G. Chigrinov, *Liquid Crystal Devices: Physics and Applications* **1999**.

45 S. Chandrasekhar, *Liquid Crystals. 2nd ed.* **1992**.

46 Carsten Tschierske, *Current Opinion in Colloid & Interface Science* **2002**, *7*, 355.

47 S. V. Pasechnik, V. G. Chigrinov, D. V. Shmeliova, *Liquid Crystals Viscous and Elastic Properties in Theory and Applications* **2009**.

48 I. G. Chistyakov, W. M. Chaikowsky, *Mol. Cryst. Liq. Cryst.* **1969**, *7*, 269.

49 A. de Vries, *Mol. Cryst. Liq. Cryst.,* **1970**, *10*, 219.

50 G. W. Stewart, *Discussions of Faraday Soc.* **1933**.

51 R. J. Birgeneau, J. D. Litster, *de Physique Lettres*, **1978**, *39*, 399. R. Pindak, D. E. Moncton, S. C. Davey, J. W. Goodby, *Phys. Rev. Lett.* **1981**. *46*, 1135.

52 A. J. Leadbetter, *in Thermotropic Liquid Crystals* **1987**.

53 P. S. Pershan, *Structure of Liquid Crystal Phases* **1988**.

54 V. K. Gupta, N. L. Abbott, *Phys. Rev. E,* **1996**, *54*, 4540.

55 J. Y. Fang, U. Gehlert, R. Shashidar, C. M. Knobler, *Langmuir* **1999**, *15*, 297.

56 V. K. Gupta, J. J. Skaife, T. B. Dubrovsky, N. L. Abbott, *Science* **1998**, *279*, 2077.

57 R. R. Shah, N. L. J. Abbott, *Am. Chem. Soc.* **1999**, *121*, 11300.

58 Y. L. Cheng, D. N. Batchelder, S. D. Evans, J. R. Henderson, J. E. Lydon, S. D. Ogier, *Liquid Crystals* **2000**, *27*, 1267.

59 Y. Y. Luk, N. L. Abbott, *Science* **2003**, *301*, 623.

60 J. Y. Fang, W. Ma, J. V. Selinger, R. Shashidhar, *Langmuir* **2003**, *19*, 2865.

61 J. M. Brake, M. K. Daschner, Y. Y. Luk, N. L. Abbott, *Science* **2003**, *302*, 2094.

62 S. V. Shiyanovskii, T. Schneider, I. I. Smalyyukh, T. Ishikawa, G. D. Neihaus, K. J. Doane, C. J. Woolverton, O. D. Lavrentovich, *Phys. Rev. E* **2005**, *71*, 020702.

63 Y. Zhao, N. Mahajan, R. Lu, J. Y. Fang, *Proc. Natl. Acad. Sci. U.S.A.* **2005**, *102*, 7438.

64 H. D. Sikes, J. T. Woodward, IV, D. K. Schawartz, *J. Phys. Chem.* **1996**, *100*, 9093.

65 K. J. Stine, S. A. Rauseo, B. G. Moore, *Phys. Rev. A* **1990**, *41*, 6884.

66 S. Akamatsu, F. Rondelez, *J. Phys. II France I* **1991**, 1309 .

67 J. Y. Fang, E. Teer, C. M. Knobler, *Phys. Rev. E* **1997**, *56*, 1859.

68 N. Mino, H. Tamura, K. Ogawa, *Langmuir* **1992**, *8*, 594.

69 G. Wegner, *Makromol. Chem*. **1972**, *154*, 35.

70 B. Tieke, G. Lieser, G. Wegner, *J. Polym. Sci., Polym. Chem.* **1979**, *17*, 1631.

71 Y. Okawa, M. Aono, *J. Chem. Phy.* **2001**, *115*, 2317.

72 K. Y. C. Lee, *Annu. Rev. Phys. Chem.* **2008**, *59*, 771.

73 X. Qiu, J. Ruiz-Garcia, K. J. Stine, C. M. Knobler, J. V. Selinger, *Phys. Rev. Lett.* **1991**, *67*, 703.

74 B**.** Fischer, M. W. Tsao, J. Ruiz-Garcia, T. M. Fischer, D. K. Schwartz, C. M. Knobler, *J. Phys. Chem.* **1994**, *98*, 7430.

75 G. Weidemann, D. Vollhardt, *Langmuir* **1996**, *12*, 5114.

76 J. Ruiz-Garcia, X. Qiu, M. W. Tsao, G. Marshall, C. M. Knobler, G. A. Overbeck, D. Mobius, *J. Phys. Chem.* **1993**, *97*, 6955.

77 D. K. Schwartz, J. Ruiz-Garcia, X. Qiu, X. J. V. Selinger, C. M. Knobler, *Physica A* **1994**, *204*, 606.

78 E. Hatta, T. M. Fischer, *Langmuir* **2002**, *18*, 6201.

79 D. K. Schwartz, M. W. Tsao, C. M. Knobler, *J. Chem. Phys.* **1994**, *101*, 8258.

80 J. Y. Fang, E. Teer., C. M. Knobler, K. K. Loh, J. Rudnick, *Phys. Rev. E* **1997**, *56*,1859.

81 J. Ignes-Mullol, J. Claret, J. F. Sagues, *J. Phys. Chem. B* **2004**, *108*, 612.

82 K. Meine, D. Vollhardt, G. Weidemann, *Langmuir* **1998**, *14*, 1815.

83 U. Gehlert, J. Y. Fang, C. M. Knobler, *J. Phys. Chem. B* **1998**, *102*, 2614.

84 K. Hisada, C. M. Knobler, *Langmuir* **2000**, *16*, 9390.

85 S. Schwiegk, T. Vahlenkamp, Y. Z. Xu, G. Wegner, *Macromolecules* **1992**, *25*, 2513.

86 J. Y. Fang, Z. H. Lu, G. W. Min, Z. M. Ai, Y. Wei, P. Stroeve., *Phys. Rev. A* **1992**, *26*,4963.

87 W. D. Harkins, E. Boyd, *J. Phys. Chem.* **1941**, *45*, 20.

88 A. D. Price, J. Ignes-Mullol, M. A. Vallve, T. E. Furtak, Y. A. Lo, S. M. Malone, D. K. Schwartz, *Soft Matter* **2009**, *5*, 2252.

89 B. Price, D. K. Schwartz, *J. Am. Chem. Soc.* **2008**, *130*, 8188.

90 J. Cognard, *Mol. Cryst. Liq. Cryst. Suppl. Ser.* **1982**, *1*, 1.

91 K. Hiltrop, J. Haase, H. Stegemeyer, *Ber. Bunsen-Ges. Phys. Chem.* **1994**, *98*, 209.

92 U. Kuhnau, A. G. Petrov, G. Klose, H. Schmiedel, *Phys. Rev. E.* **1999**, *59*, 578.

93 S. F. Yu, H. L. Zhou, P. S. He, *J. Mat. Sci.* **1999**, *34*, 3149.

94 S. P. Wang, J. Ramirez, Y. S. Chen, R. M. Lenblanc, *Langmuir* **1999**, *15*, 5623.

95 K. Ogawa, *J. Phys. Chem.* **1989**, *93*, 5305.

96 C. A. J. Putman, H. G. Hansma, H. E. Gaub, P. K. Hansma, *Langmuir* **1992**, *8*, 3014.

97 C. Gourier, M. Alba, A. Braslau, J. Daillant, M. Goldmann, C. M. Knobler, F. Rieutord, G. Zalczer, *Langmuir* **2001**, *17*, 6496.

98 B. M. Goettgens, R. W. Tillmann, M. Radmacher, H. E. Gaub, *Langmuir* **1992**, *8*, 1768.

99 A. Lio, A. Reichert, D. J. Ahn, J. O. Nagy, M. Salmeron, D. H. Charych, *Lanmuir* **1997**, *13*, 6524.

100 C. Gourier, C. M. Knobler, J. Daillant, D. Chatenay, *Langmuir* **2002,** *18,* 9434.

101 S. P. Wang, R. Lunn, M. P. Krafft, R. M. Leblanc, *Langmuir* **2000**, *16*, 2882.

102 M. P. Valignat, S. Villette, J. Li, R. Barberi, et al. *Phy. Rev. Lett.* **1994**, *77*, 10.

103 A. G. Petrov, A. Derzhanski, *Mol. Cryst. Liq. Cryst. Lett*. **1977**, *41*, 41.

104 P. G. de Gennes, J. Prost, *The Physics of Liquid Crystals, 2nd ed.* **1993.**

105 M. Kleman, O. D. Lavrentovich, *Soft Matter Physics: An Introduction 1st ed.* **2003.**

106 T. Shirakawa, T. Inoue, T. Tokuda, *J. Phys. Chem.* **1982**, *86*, 1700.

107 D. L. Patrick, T. P. Beebe Jr., *Langmuir* **1994***, 10*, 298.

108 Z. Zhang, DS. Zheng, Y. Guo, HF. Wang, *Phy. Chem. Chem. Phys.* **2009**, *11*, 991.

109 J. Z. Xue, C. S. Jung, M. W. Kim, *Phys. Rev. Lett.* 1992, *69*, 474.

110 C. S. Mullin, P. Guyot-Sionnest, Y. R. Shen, *Phys. Rev. A* **1989**, *39*, 3745.

111 J. Y. Huang, R. Superfine, Y. R. Shen, *Phys. Rev. A* **1990**, *42*, 3660.

112 M. Barmentlo, F. R. Hoekstra, N. P. Willart, R.W. Hollering, *J. Phys. Rev. A* **1991**, *43*, 5740.